NASA TECHNICAL MEMORANDUM

NASA TM X-1655

BLOCKAGE EFFECTS OF CONE-CYLINDER BODIES ON PERFORATED WIND TUNNEL WALL INTERFERENCE

by Glenn A. Mitchell

Lewis Research Center
Cleveland, Ohio

NATIONAL AERONAUTICS AND SPACE ADMINISTRATION • WASHINGTON, D. C. • OCTOBER 1968

NASA TM X-1655

BLOCKAGE EFFECTS OF CONE-CYLINDER BODIES ON PERFORATED WIND TUNNEL WALL INTERFERENCE

By Glenn A. Mitchell

Lewis Research Center
Cleveland, Ohio

NATIONAL AERONAUTICS AND SPACE ADMINISTRATION

For sale by the Clearinghouse for Federal Scientific and Technical Information
Springfield, Virginia 22151 – CFSTI price $3.00

ABSTRACT

A variety of cone-cylinder models were tested in the Lewis 8- by 6-Foot Supersonic Wind Tunnel at speeds from Mach 0.5 to 2.0 to evaluate the effect of wall-reflected disturbances on model pressure distributions. In all cases, a 10^{o} half-angle conical forebody was used; and the cylinder diameter was varied from 4 inches (10.16 cm) to 16 inches (40.64 cm). There were additional variations in model position within the test section and also in tunnel wall porosity.

BLOCKAGE EFFECTS OF CONE-CYLINDER BODIES ON PERFORATED WIND TUNNEL WALL INTERFERENCE

by Glenn A. Mitchell

Lewis Research Center

SUMMARY

A variety of cone-cylinder models were tested in the Lewis 8- by 6-Foot Supersonic Wind Tunnel at speeds from Mach 0.5 to 2.0 to evaluate the effect of wall-reflected disturbances on model pressure distributions. In all cases, a 10^{o} half angle conical forebody was used; and the cylinder diameter was varied from 4 inches (10.16 cm) to 16 inches (40.64 cm). There were additional variations in model position within the test section and also in tunnel wall porosity. Principal disturbances were identified as: (1) flow acceleration at the rear of the test section at subsonic speeds, (2) decrements in nose cone pressures at sonic speed, (3) displacement of the terminal shock near sonic speeds, (4) excessive wall porosity near sonic speeds, and (5) anomalies resulting from nonuniform distribution of tunnel wall porosity. As expected, these disturbances increased as the model blockage increased.

INTRODUCTION

As discussed in reference 1, a transonic wind tunnel design is a judicious compromise of conflicting desires and requirements resulting from the mutual interaction of the test model flow field and the tunnel walls. With a given tunnel design, there is a continuing motivation to utilize test models which are as large as possible without incurring serious compromises in flow quality. In some cases (e.g., aircraft aerodynamic force tests) only minor compromises can be permitted. But in other cases, major compromises may be essential or else tunnel test plans must be abandoned simply because the model is too small. Some examples of the latter situation include structural tests of full-scale components of flight vehicles, dynamic tests of aeroelastic models of flight vehicles, model tests of complex variable geometry aircraft inlet and exhaust systems, or model tests wherein mixing and/or combustion phenomena are of fundamental interest

as in rocket launch vehicle base heating studies or airbreathing engine tests.

In interpreting results of tests requiring the use of large models, a general knowledge of the deviations in flow quality is needed to avoid inaccurate conclusions. However, only limited data are published defining the consequences of using large models in transonic tests. For this reason, a series of calibration models have been tested in the Lewis 8- by 6-Foot Supersonic Wind Tunnel over its speed range from Mach 0.5 to 2.0. Although some details of the results may be peculiar to the particular tunnel in which the tests were made, general trends may be expected to exist also in other transonic tunnels of similar design.

SYMBOLS

M Mach number

p static pressure

P total pressure

Δ deviation

Subscript:

0 free-stream conditions

APPARATUS AND PROCEDURE

Considerations in Varying Test Section Porosity

The 8- by 6-Foot Supersonic Wind Tunnel was originally constructed as a supersonic tunnel for operation in the speed range Mach 1.5 to 2.0. Subsequently, the test section walls were perforated to permit transonic operation. The perforation design was based on the differential resistance concept of reference 2. One inch diameter holes were drilled in the tunnel wall 60° from the normal to provide greater resistance to inflow than to outflow and thereby minimize the strength of wall-reflected disturbances from the model flow field. General arrangement of the test section equipment is illustrated in figure 1(a). In this particular tunnel, the perforations are arranged in a herringbone pattern (indicated in fig. 1(b)) which is inclined 75° to the flow direction and is symmetrical about the center of each wall.

Although the objective in design of the wall perforations was to provide a uniform porosity of 6 percent over a 14-foot length, existing support structure limited hole placement and resulted in large wall areas without porosity. This is illustrated in

figure 1(b) which is a representation of the test section side wall. The lined areas represent the perforated areas. Although the average porosity of 5.8 percent was close to the design value, nearly 50 percent of the wall area was unperforated and local porosity in the perforated area was 11.2 percent. The resulting longitudinal porosity variation is shown by the upper curve of figure 2.

The initial test runs revealed that large flow disturbances were created by the solid (or unperforated) side wall area centered about tunnel station 5 (figs. 1(b) and (2). This information resulted in the inclusion of limited test section modifications into the test program in an effort to eliminate or reduce the disturbance. One approach was to shorten the perforated test section to 8 feet (2.44 m) (fig. 2). Another approach was to reduce porosity and thus reduce the porosity differential across the unperforated areas. A test section of reduced porosity was also suggested by the fact that the local porosity of 11.2 percent was almost twice the average porosity of 5.8 percent. Local porosity is of concern because, except for a few support structure locations, the centerline regions of both the horizontal and vertical tunnel walls were fully perforated plates. It is these centerline regions that would reflect uncancelled model flow field pressures directly back to the model as a disturbance. It had been assumed in the tunnel design that average porosity was the major factor controlling wall flow characteristics rather than local porosity. The 6 percent design criterion, however, originated in a transonic tunnel having uniformly-perforated walls or walls in which local porosity and average porosity were identical (ref. 2). Thus the alternate assumption, that local porosity is the major factor controlling wall flow characteristics, may be more valid and would require the local porosity of the 8- by 6-foot walls to be reduced to 6 percent and the average porosity to 3 percent.

Three different test section configurations are currently used in model testing. These three test sections, whose porosity variations are shown in figure 2, are the 14 foot (4.27 m) - 5.8 percent porosity test section and two shorter test sections - the 8 foot (2.44 m) - 6.2 percent porosity and the 8 foot (2.44 m) - 3.1 percent porosity test sections. The shorter test section was created from the 14-foot (4.27 m) test section by plugging all holes in the forward part of the tunnel. Thus, the 8 foot (2.44 m) - 6.2 percent porosity test section is simply the aft portion of the 14 foot (4.27 m) - 5.8 percent porosity test section; the variation in average porosity resulting from different amounts of unperforated areas. Local porosity was the same in both test sections. The low porosity test section was achieved by plugging every other hole in the 8 foot (2.44 m) - 6.2 percent porosity test section, thereby reducing the average porosity to 3.1 percent and the local porosity to 5.6 percent.

Considerations in Selecting a Test Model

A determination of the tunnel flow quality could best be accomplished by comparing experimental pressure distributions obtained from a test body in the tunnel to theoretical or free-flight pressure distributions. Such a comparison would determine tunnel-originated disturbances and would measure the test section capability to handle supersonic and transonic interference phenomena. The effect of model blockage on interference phenomena could be determined by testing models of various sizes.

Theoretical pressure distributions for cone cylinders of 5°, 10°, and 15° half-angles had been computed by the method of characteristics in reference 3 for supersonic Mach numbers as low as 1.3. The 10° cone appeared to be a better choice over the 15° cone since its conical shock wave would remain attached at lower supersonic Mach numbers. Hence, theoretical pressure distributions could be obtained at these lower speeds by assuming that the Taylor-Maccoll theory (upon which the calculations of reference 3 were based) was still valid since the shock wave was still attached. The 5° half-angle cone was considered too slight to test the tunnel wall shock cancellation capabilities. Accordingly, a 10° half-angle cone-cylinder was selected as the optimum body shape; and the corresponding calculations of reference 3 were extrapolated to Mach number 1.1 to provide theoretical data over the complete supersonic Mach number range of the tunnel. At a Mach number of 1.0, no theoretical data exist; and unpublished interference-free pressure distributions were selected from several sources and combined to compare with the experimental tunnel data. No experimental or theoretical data were available for the subsonic speed range.

The cone-cylinder models used in these tests were sting mounted at approximately the two model nose locations shown in figure 1. The forward location was used when testing in the 14-foot (4.27 m) test section and the rear location in the 8-foot (2.44 m) test sections. Model diameters of 4, 8, 12, and 16 inches (10.16, 20.32, 30.48, and 40.64 cm) were used during the tests. A schematic drawing of the various test models showing the diameter, length, and position of each model used in each test section configuration is shown in figure 3. Models tested in the 14-foot test section are about 3 feet longer than the models in the short test sections. Except for the 4-inch (10.16 cm) diameter models, the base location of all models is approximately the same. The percent blockage (model cross-sectional area ratioed to test section flow area) of each diameter model and the length of each tested combination of model and test section is presented in table I.

Instrumentation

All test models were instrumented with a row of static pressure taps in both the

horizontal and the vertical planes of the model. The taps were generally 2 inches (5.08 cm) apart but were spaced as close as 1 inch (2.54 cm) immediately aft of the cone shoulder.

A longitudinal row of static pressure taps along the tunnel side wall and top wall was used as an aid in tracing and interpreting the various disturbances revealed by the model pressures. Selected static pressures along the tunnel top wall were averaged and ratioed to tunnel total pressure to compute test section Mach number. Care was exercised to assure that the selected static pressures were forward of any discrete model pressure disturbances that existed at supersonic speeds. Total pressure was measured in the tunnel bellmouth forward of the flexible nozzle and was corrected by a previously-calibrated loss factor to obtain the test section total pressure.

For future tests in the transonic test section, it was desirable to eliminate the dependency of test section Mach number on tunnel static pressure measurements, because with blunt bodies at low supersonic speeds no test section static pressure would be free of model disturbances. Therefore, the pressure in the plenum chamber surrounding the test section was measured and ratioed to the total pressure for each Mach number and each test section configuration to serve as a means of controlling Mach number in future tests.

Selection of Optimum Operating Conditions

The Mach number in the transonic test section of the tunnel was varied during these tests from 0.55 to 2.0 in approximate intervals of 0.1 Mach number by proper setting of four controls; compressor speed, flexible nozzle position, plenum chamber suction, and second throat position. In the supersonic speed range (Mach 1.1 to 2.0), the second throat was positioned open and the compressor speed was governed by a requirement of sufficient pressure ratio for supersonic flow. The flexible nozzle was used to set the Mach number entering the perforated test section. Vernier adjustments to the Mach number within the perforated test section were made by varying the plenum chamber suction flow rate to obtain a series of data points in each 0.1 Mach number interval. These data were used to select (on the basis of the best body pressure distributions) the optimum plenum pressures for each test section configuration. The data presented herein are the closest available test points to these optimum conditions. At subsonic speeds, the flexible nozzle was not a useful variable and was left in a wide-open position. Plenum chamber flow rate, second throat position, and compressor speed were all capable of varying the subsonic Mach number. However, a parametric study of the effect of these three variables on subsonic flow was not possible because it was necessary to set them at almost unique values at each Mach number in order to prevent unloading

of the last stages of the compressor and overpressurization of the plenum chamber surrounding the test section.

DISCUSSION OF RESULTS

Zero degree angle-of-attack pressure distributions obtained on the model bodies for all configurations shown in table I are presented in figures 4 through 12. Data are shown in order of ascending Mach number over the complete speed range investigated for each configuration. At the subsonic Mach numbers where no theory is available for comparison, the tunnel static pressure level is shown at the end of each pressure distribution. At Mach numbers of one and above, the free-flight and theoretical pressure distributions are shown as faired solid lines.

Major Flow Disturbances

All major flow disturbances were traceable to a known source. Those occurring at supersonic Mach numbers are identified and labeled on the pressure distributions of figures 4 through 12. The magnitude of each identified disturbance was obtained from these pressure distributions for later presentation. In the sonic to supersonic Mach number range, where free-flight or theoretical model pressure distributions were available, the magnitude of a pressure disturbance was simply defined as the deviation in experimental pressure above or below the theoretical or free-flight curve. At subsonic Mach numbers, no discrete tunnel disturbances existed except for pressure decreases caused by tunnel flow acceleration near the downstream end of the test section.

Subsonic flow acceleration. - At all subsonic Mach numbers, the test models with base locations near the aft end of the test section experienced a pressure decrease near the model base in excess of the normal decrease resulting from flow expansion around the base edge. This was a result of flow acceleration (or pressure drop) at the downstream end of the test section (caused by boundary layer effects on the perforations) and is illustrated by any of the subsonic pressure distributions in figures 6 through 12. Figures 4 and 5 illustrate the more normal decrease which was obtained with the model forward of the acceleration effect. Limiting the model base to 50 inches (1.27 m) from the end of the test section effectively eliminated the tunnel-induced model pressure drop. Each of the subsonic model pressure distributions in figures 4 through 12 was scanned for the point that limited this pressure drop to 1 percent of total pressure. This limit was found for the various test sections to be as far as 48 to 54 inches (1.22 to 1.37 m) upstream from the end of the test section as is shown in figure 13. The base location of

each model is also shown in the figure. When the model base was positioned forward of the flow acceleration effect, as was done with the 4-inch (10.16 cm) model (figs. 13(a) and (c)), a pressure drop still resulted. However, the pressure drop did not vary with Mach number and remained very close to the model base, indicating that the effect was not due to tunnel flow acceleration but to expansion of the subsonic flow around the sharp end of the model. Thus, subsonic pressure drops shown for the 4 inch (10.16 cm) models in the pressure distributions of figures 4 and 5 are, in reality, true model flow effects.

The flow acceleration exhibited by the tunnel at the aft end of the perforated test section is not an effect limited to this particular facility. Acceleration as well as deceleration at subsonic speeds near the end of a perforated test section was predicted by Goethert (ref. 4) on theoretical grounds and has been demonstrated experimentally in other facilities (refs. 5 and 6). The acceleration can be explained as an effect of tunnel boundary layer upon the flow characteristics of the perforations. In the case of flow acceleration, the amount of exhauster suction (and mass flow through the wall) is small and the tunnel boundary layer thickens longitudinally to the extent that, near the aft portion of the test section, the natural resistance of the perforations to inflow is reduced until low energy air enters the test section in increasing amounts, thickens the boundary layer, and causes a sufficient constriction of flow area to accelerate the flow. As may be imagined, control of exhauster suction (or boundary layer growth) at a given subsonic speed could be used to largely eliminate this disturbance. Such a technique, similar to that reported in reference 6, has been developed for the 8- by 6-foot Supersonic Wind Tunnel in subsequent tests. Variable wall divergence has also been used in some tunnels with limited success to control this disturbance but was not applicable in this facility since the walls are fixed in parallel positions.

Transonic interference effects on model forebody. - At a Mach number of one, the cone pressures obtained on all models in figures 4 through 12 were depressed below the free-flight values. The maximum decrement measured for each configuration (plotted in fig. 14) seemed quite small with a maximum value of about 2 percent of total pressure. The increase of the decrement with model size was an expected result inasmuch as the effect is a result of model blockage and is caused by a transonic interference field over the conical portions of the model (ref. 7). The net effect of the interference is a delay in the rise of the vehicle drag curve approaching Mach number one, and the resulting errors in measured drag can be quite large.

The terminal shock. - Transonic tunnel wall interference also affects the terminal shock. In free flight, the terminal shock forms in the flow field of a body as the subsonic velocity increases toward sonic speed. Formation generally occurs between the subsonic Mach numbers of 0.90 and 0.96. Specifically, the Mach number required is such that flow over part of the body surface is accelerated to local supersonic speeds in excess of about Mach number 1.1 (ref. 8). This supersonic region is generally terminated by a

shock to satisfy the downstream boundary conditions. As the flight velocity increases, the terminal shock rapidly moves aft and disappears downstream at, or slightly above, Mach number one. In the presence of a tunnel wall, however, the flow field about a relatively large blockage body is radically altered and so is the terminal shock location. According to reference 7, the location of the terminal shock is believed to be linked to the intersection of the expansion field from the model with the tunnel walls. The effect of the terminal shock on model pressure distributions is best illustrated in figure 8. The longitudinal progression of this disturbance can be traced from Mach number 0.891 to 1.275. In figure 15, the terminal shock location in model diameters from the cone shoulder is plotted as a function of Mach number for each model size tested. The curve for the 0.005 percent blockage model was obtained from Schlieren photographs in reference 7 and was presumed to be representative of flight. As the model blockage was increased, the terminal shock moved aft less rapidly with increasing Mach number.

With the 1.64 and 2.91 percent blockage models, the terminal shock was located forward of the Mach one free-flight position even at a supersonic Mach number of 1.25. All of the models tested were too large to simulate the free-flight terminal shock location except at Mach numbers near 0.9. Elimination of this disturbance at Mach numbers above 1.1 could easily be accomplished with the 4-inch (0.18-percent blockage) model by placing the base upstream of the terminal shock location at Mach number 1.1. Such a model length is reasonable. The same technique is inapplicable to the larger models because it quickly leads to unreasonably short models (in terms of diameters) not only at Mach number 1.1 but also at 1.2. Effectively this length limitation may limit the diameter of a scale model if the terminal shock position has an important bearing on the desired results of the test. Changing the test section from 14 foot (4.27 m) - 5.8 percent porosity to 8 foot (2.44 m) - 6.2 percent porosity had no effect on terminal shock location. The only test section effect was due to porosity variation. The 5.8 or 6.2-percent porosity walls retarded the shock movement of the larger models slightly more than did the 3.1 percent porosity walls.

Inasmuch as the location of the terminal shock was in error on all models and at all Mach numbers except 0.9, the disturbance produced by the shock must be presumed to be a disturbance not representative of interference free flow. On the other hand, the terminal shock disturbance exhibited at Mach number 0.9 by all models was considered to represent free-flight because the lack of shock movement with changes in model blockage suggested a lack of flow interference.

The effect of model blockage on terminal shock magnitudes is shown in figure 16 for Mach numbers of 1.0 and above. With the larger models of 2.91 and 1.64 percent blockage, shock magnitudes of 8 to 10 percent of total pressure were observed at sonic speed. Generally, these magnitudes decreased as the Mach number was increased but still exceeded about 4 percent for these models at the highest observed Mach number.

In general, the shock magnitudes decreased with reductions in model size. The smallest model (0.18-percent blockage) was clearly superior to other models in limiting maximum shock magnitudes to about 3 percent of total pressure.

A replot of the data of figure 16 is presented in figure 17 showing the effect of various test sections on the terminal shock magnitude. Although a reduction in shock magnitude was obtained by shortening the test section from 14 to 8 feet (4.27 to 2.44 m) and by reducing porosity from 6.2 to 3.1 percent, the amount of reduction was minimal at Mach number 1.0. At Mach numbers near 1.1, however, shortening the test section reduced shock magnitudes as much as 4 percent of total pressure and reducing porosity lowered magnitudes as much as 5 percent. Thus, for the 8 foot (2.44 m) - 3.1 percent porosity test section, maximum terminal shock magnitudes at Mach number 1.1 were limited to 4 percent of total pressure whereas with the other test sections, maximum values were in excess of 8 percent.

Excessive wall porosity at Mach number 1.1. - The model nose shock was notably absent from the disturbances identified on the model pressures of figures 4 through 12. Only an occasional model pressure disturbance was traceable to the model nose shock when the shock fell in a perforated section of the tunnel. The magnitude of the disturbance in this event was within the general data scatter. These perforated walls, having local porosities of 11.2 and 5.6 percent, were also effective in minimizing wall reflections of the rest of the body flow field over most of the supersonic Mach number range. Perforated wall reflections of the nose cone compression field and the cone shoulder expansion field were not discernable from the pressure distributions (figs. 4 through 12) except near Mach number 1.1. At this Mach number, the nose cone compression field was reflected from the wall to the model as an expansion. An example of this is illustrated by the Mach 1.099 pressure distribution of figure 6(g). The magnitude of this expansion was generally about 4 to 5 percent of total pressure as shown in figure 18. Thus, the walls were acting as an over-corrective boundary causing excessive flow turning or over-expansion at the wall and acting much like a free jet to the model nose compression field. This suggests that a reduction in porosity at this Mach number of 1.1 would improve the wall characteristics by limiting outflow. The previously discussed reduction in terminal shock intensity and displacement, realized by lowering local wall porosity, also suggests that the flow could be improved by a smaller porosity wall. Indeed, such a result was achieved by the variable porosity test section presented in reference 9 which reported 5.4-percent porosity walls were best except around Mach number 1.1 where porosities as low as 0.5 percent resulted in excellent flow.

Unperforated side wall near tunnel station 5. - A disturbance originating from the unperforated region in the 14-foot (4.27 m) test section sidewall at about station 5 (see fig. 2) and propagating from the wall to the model at the Mach angle was observed from Mach numbers of about 1.2 to 1.97. The disturbance was particularly severe at Mach numbers from 1.2 to 1.37 as shown in figure 8. The magnitude of the pressure distur-

bance caused by the unperforated area is presented in figure 19. Variations in model size from 0.18 to 2.91 percent blockage had little effect on the disturbance magnitudes. At Mach numbers above 1.5, the disturbance level was low and ranged from 1 to 2 percent of total pressure. At these high speeds, the model nose shock was downstream of the unperforated sidewall region. At lower speeds, the nose shock and the cone compression field were reflected from the unperforated region and resulted in a concentrated disturbance as high as 4 to 5 percent of total pressure at Mach number 1.2. As the speed was lowered from Mach number 1.2 to 1.1, the disturbance entirely disappeared. Two events contributed to this effect: the nose shock moved forward of the unperforated area, and the top and bottom perforated tunnel walls reflected the nose cone pressure field as an expansion that completely negated the compression field reflected from the unperforated side wall.

Unperforated side wall near tunnel station 9.5. - The porosity deficit region at tunnel station 9.5 illustrated in figure 2 is shown in figure 1 to be a short region without perforations. A disturbance from this region was observed propagating along the Mach angle to the model from both the tunnel horizontal and vertical (side) walls. This is illustrated for the 12-inch (30.48 cm) model in the short (8 foot) (2.44m) test section in figure 10 from Mach numbers of 1.1 to 1.56. This disturbance can be identified at higher Mach numbers with a longer model in the 14-foot (4.27 m) test section (fig. 11). Presented in figure 20 are the magnitudes of the pressure disturbances caused by the unperforated wall section at tunnel station 9.5. Disturbance magnitudes over the supersonic Mach number range are compared for the various size models in each test section. The curves of figure 20 terminate at various upper Mach numbers as the disturbance moved aft of the model base. The maximum disturbance from the unperforated area was 4 to 5 percent of total pressure and occurred at about Mach number of 1.2 for the larger blockage models. In general, a reduction in model blockage, or diameter, reduced the disturbance magnitude. The greatest benefit of reduced blockage occurred in the low supersonic speed range (Mach number 1.1 to 1.3). For example, reducing blockage from 1.64 to 0.73 percent lowered the disturbance magnitude by 3 percent. Actually this benefit was due to the decrease in the extent of the model nose cone compression field resulting from the smaller model. With the larger models, the nose cone pressure field was reflected from the unperforated region in the lower supersonic speed range. But with smaller models (for example, the 8-inch (20.32 cm) model in the 8-foot (2.44 m) test section and the 12-inch (30.48 cm) model in the 14-foot (4.27 m) test section) the nose cone compression field moved forward of the unperforated region as the Mach number was reduced from 1.35 and thus reduced the disturbance. The 0.18 percent blockage model is not shown in figure 20 because the disturbance was downstream of the base of this short model and was therefore zero.

The data from figure 20 was replotted to show a comparison of the effect of various test sections on the disturbance from station 9.5 and is presented as figure 21. A reduc-

tion in porosity from 6.2 to 3.1 percent in the 8-foot (2.44 m) test section resulted in a slight increase of about 1 percent in the magnitude of the disturbance from the unperforated region (figs. 21(b) and (c)). Thus, a reduction in porosity variation across an unperforated region by lowering overall porosity does not reduce the pressure disturbance from that region. Inasmuch as the disturbance magnitudes from the unperforated region at station 9.5 were very dependent on impingement of the model flow field, a valid comparison between the 14-foot (4.27 m) and 8-foot (2.44 m) test sections can be made only at Mach numbers which propagate similar model flow fields to the unperforated region. Such a Mach number range was found in two cases: between Mach numbers of 1.35 and 1.55 for the 12-inch (30.48 cm) model and between Mach numbers of 1.2 and 1.35 for the 16-inch (40.64 cm) model. In both instances the disturbance magnitudes in the 14-foot (4.27 m) and 8-foot (2.44 m) test sections were within 1 percent of each other. Thus, no test section modification was successful in suppressing the disturbance from the unperforated region at tunnel station 9.5.

Flow Disturbance Magnitudes

The magnitude of the maximum model surface pressure disturbance was obtained from each pressure distribution in figures 4 through 12 and plotted in figure 22 as a function of Mach number so as to compare the effects of model diameter (or blockage) on the flow quality in each test section. The magnitude of the subsonic disturbance (as plotted in fig. 22) was defined as the pressure deviation below free-stream static pressure exhibited near the base of each model. Thus, the values plotted subsonically in figure 22 contain model base effects as well as tunnel effects. Although the model sting diameter varied from 0.4 of the base diameter with the 4- and 8-inch (10.16 and 20.32 cm) models to 0.2 with the 16-inch (40.64 cm) model, the effects were small and did not mask the tunnel effects. With most configurations of model and test section, the largest pressure disturbances were observed at Mach numbers from 0.8 to 1.0. As the Mach number was decreased or increased from this speed range, the disturbance magnitudes were rapidly reduced. Above a Mach number of 1.6, all major disturbances were reflected aft of the models in the 8-foot (2.44 m) test sections (figs. 22(b) and (c)); hence, pressure deviations were slight (about 1 percent of total pressure).

Although the data exhibit some scatter, reducing the model size or blockage substantially lowered the magnitude of the model surface pressure disturbances. The peak disturbance magnitudes of 10 to 12 percent observed with the largest model (2.91 percent blockage) were reduced to about 4 percent of total pressure by limiting the model blockage to 0.18 percent. Had the scale lengths of both models been identical, greater reductions

might have resulted inasmuch as the smallest model was 7 to 14 diameters longer than the largest model (see table I).

The data of figure 22 have been replotted in figure 23, comparing the effect of the different test sections on the maximum pressure disturbance magnitudes for each model size. From the standpoint of minimum model pressure disturbance, the 14 foot (4.27 m) - 5.8 percent porosity test section was inferior to the 8-foot (2.44 m) test sections. A considerable reduction in pressure disturbances (up to 4 percent of total pressure) was obtained in the low supersonic speed range about Mach number 1.1 by shortening the tunnel to the 8 foot (2.44 m) - 6.2 percent porosity test section. A further reduction was obtained by changing the test section porosity to 3.1 percent. This resulted in reductions of up to 5 percent. At subsonic speeds, the pressure decrease due to flow acceleration at the rear of the test section was reduced on the intermediate sized models (8- and 12-inch) (20.32 and 30.48 cm) when the test section was shortened and the porosity reduced.

Another comparison of the effect of using different test sections is presented in figure 24 showing only pressure disturbances that occurred within the first 57 inches (145 cm) of model length. Such a comparison eliminates consideration of the subsonic pressure drop at the rear of the test section; and, therefore, only data obtained at supersonic speeds are presented. Effectively, all models became the same length as the short 4-inch (10.16 cm) diameter model shown in figure 3. Under these conditions, many disturbances now fell downstream of the models. In fact, this length was chosen to eliminate the disturbance from the unperforated wall at tunnel station 9.5 and provide flow without a major disturbance at Mach numbers of 1.2 and above. As illustrated in figure 24, this goal was realized in the 8-foot (2.44 m) test sections, which limited disturbances above Mach number 1.1 to 2 percent of total pressure. The higher disturbance magnitudes at Mach number 1.1 and below resulted from the terminal shock displacement which cannot be corrected. The same limited length models in the 14-foot (4.27 m) test section could not eliminate the disturbance from the unperforated side wall region at tunnel station 5 simply because of its relative position. This disturbance was evident at low supersonic Mach numbers and exhibited a magnitude of 5 percent (fig. 24). Thus, a considerable improvement in tunnel flow quality was obtained by eliminating the effects of unperforated wall areas. This was accomplished, however, only by the rather drastic action of eliminating as usable test section the forward 6 feet (1.83 m) of the 14-foot (4.27 m) perforated length and shortening the models to exclude from use the last 50 inches (1.27 m) of test section. Also noted with these short models was the superiority of the lower porosity test section as evidenced by a small (about 1 percent), but consistently lower, pressure deviation at the low supersonic speeds.

SUMMARY OF RESULTS

Pressure distributions on four 10^{o} half-angle cone-cylinder models ranging in size from 4 inches (10.16 cm) to 16 inches (40.64 cm) in diameter (0.18 to 2.91 percent blockage) were obtained in the three currently used 8- by 6-Foot Supersonic Wind Tunnel test section configurations and compared with available theoretical and free-flight pressure distributions to determine the flow quality produced with each configuration. Results and observations are as follows:

1. A variety of specific flow disturbances of major proportions were discovered. These affected the flow quality of most of the configurations. These disturbances were:
   (a) A model pressure decrease at subsonic tunnel velocities caused by aft test section flow acceleration.
   (b) A decrement in model nose cone pressures at sonic speed caused by wall interference with the transonic flow field.
   (c) A displacement of the terminal shock near sonic speeds caused also by transonic interference.
   (d) Overexpansion of the cone flow field at a Mach number of 1.1 resulting from an overeffective wall porosity.
   (e) A pressure disturbance at supersonic speeds from an unperforated tunnel sidewall area at tunnel station 5 in the 14-foot (4.27 m) test section.
   (f) A pressure disturbance at supersonic speeds from an unperforated wall area at tunnel station 9.5.
2. Model surface pressure distributions were perturbed most strongly near sonic speeds.
3. Sufficient reduction in model size considerably improved model flow quality (reduced disturbances).
4. Shortening the 14-foot (4.27 m) test section to 8 feet (2.44 m) also improved flow quality. A substantial part of this improvement resulted from elimination of the disturbance from the unperforated sidewall near station 5.
5. A further improvement in model surface pressure distributions (or flow quality) was obtained by reducing tunnel wall porosity. However, even though reduced wall porosity lessened the porosity variation across the unperforated region at station 9.5, the disturbance from that station was not reduced.

Lewis Research Center,
National Aeronautics and Space Administration,
Cleveland, Ohio, April 29, 1968,
126-15-02-10-22.

REFERENCES

1. Goethert, Bernhard H.: Transonic Wind Tunnel Testing. AGARDograph No. 49, Pergammon Press, 1961.

2. Gray, J. Don; and Gardenier, Hugh E.: Experimental and Theoretical Studies on Three-Dimensional Wave Reflection in Transonic Test Sections. Part I. Wind-Tunnel Tests on Wall Interference of Axisymmetric Bodies at Transonic Mach Numbers. Aro, Inc. (AEDC TN-55-42), Mar. 1956.

3. Clippinger, R. F.; Giese, J. H.; and Carter, W. C.: Tables of Supersonic Flows About Cone cylinders. Part I: Surface Data. BRL Rep. No. 729, Aberdeen Proving Grounds, July 1950.

4. Goethert, B. H.: Flow Establishment and Wall Interference in Transonic Wind Tunnels. Aro Inc. (AEDC TR-54-44), June 1954.

5. Chevalier, H. L.: Calibration of the PWT 16-Foot Transonic Circuit With a Modified Model Support System and Test Section. Aro, Inc. (AEDC TN-60-164), Aug. 1960.

6. Nichols, James H.: Determination of Optimum Operating Parameters for the PWT 16-Foot Transonic Circuit Utilizing One-Percent Bodies of Revolution. Aro. Inc. (AEDC TN-59-100), Sept. 1959.

7. Page, William A.: Experimental Study of the Equivalence of Transonic Flow About Slender Cone-Cylinders of Circular and Elliptic Cross Section. NACA TN 4233, 1958.

8. Sinnott, Colin S.: On the Prediction of Mixed Subsonic/Supersonic Pressure Distributions. J. Aero/Space Sci., vol. 27, no. 10, Oct. 1960, pp. 767-778.

9. Felix, A. Richard: Variable Porosity Walls for Transonic Wind Tunnels. Presented at the 22nd Semi-Annual Meeting of the Supersonic Tunnel Association, Brussels, Belgium, Sept. 1964.

TABLE I. - MODEL AND TEST SECTION CONFIGURATIONS

Model diameter		Model blockage, percent	Test section								
			14 ft (4.27 m); 5.8 percent porosity			8 ft (2.44 m); 6.2 percent porosity			8 ft (2.44 m); 3.1 percent porosity		
			Model length								
in.	cm		in.	cm	diam	in.	cm	diam	in.	cm	diam
4	10.16	0.18	86.3	219.2	21.6	----	-----	----	57.4	145.8	14.3
8	20.32	0.73	----	-----	----	86.4	219.5	10.8	86.4	219.5	10.8
12	30.48	1.64	120.9	307.1	10.1	84.9	215.7	7.1	84.9	215.7	7.1
16	40.64	2.91	120.9	307.1	7.6	86.4	219.5	5.4	----	-----	---

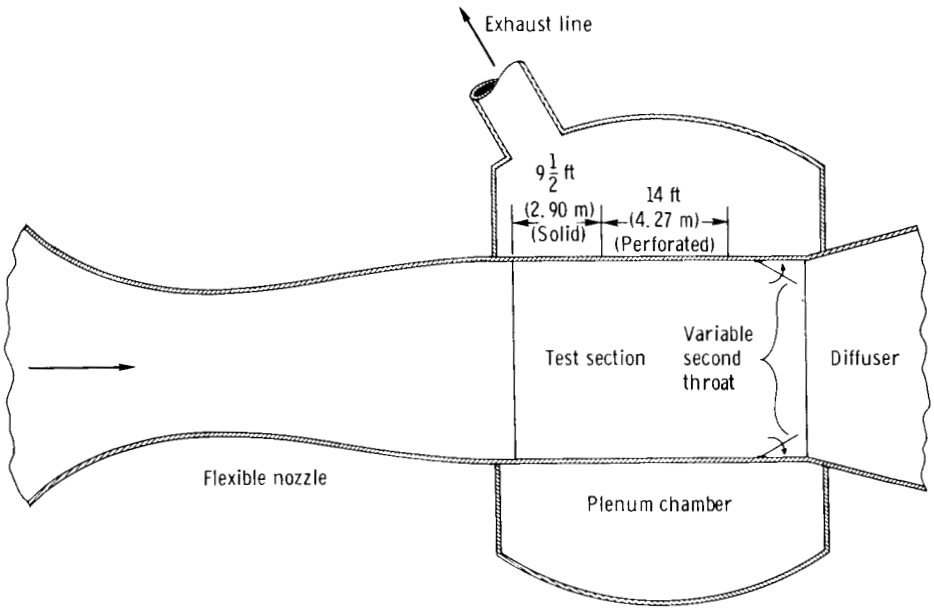

(a) Schematic drawing of test section and associated equipment.

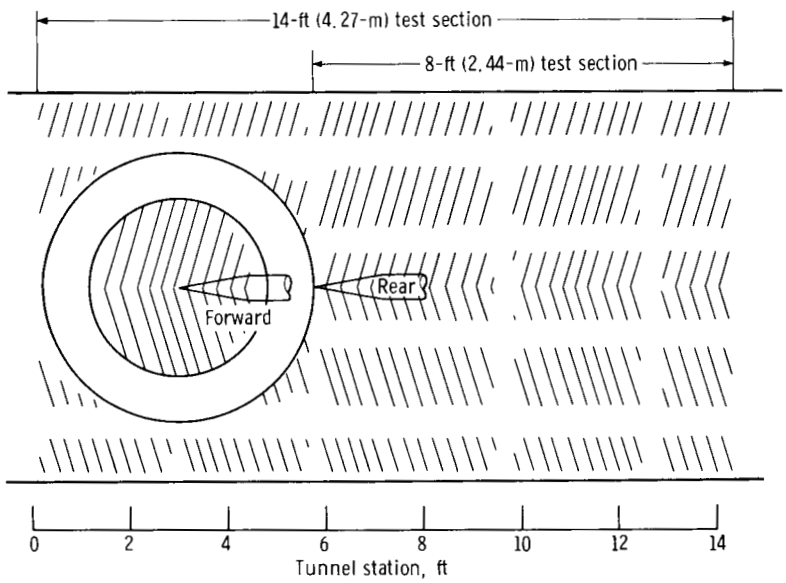

(b) Sidewall perforations.

Figure 1. - The 8- by 6-Foot Supersonic Wind Tunnel test section design.

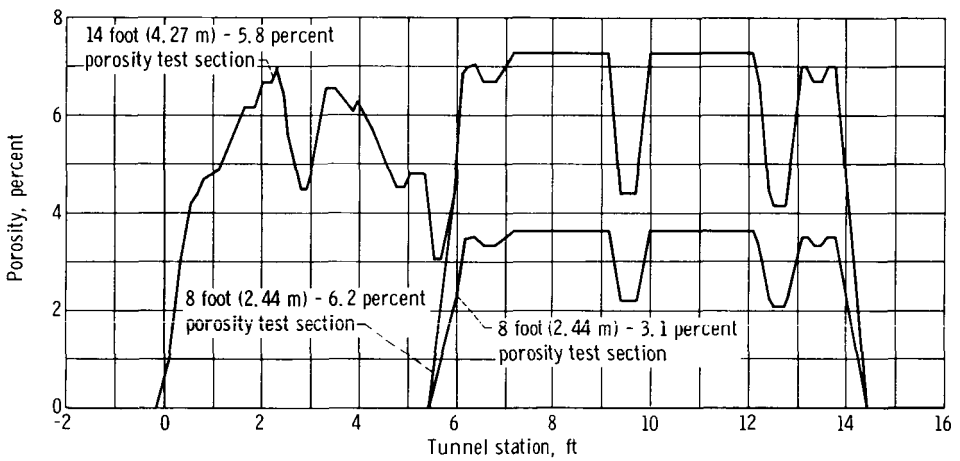

Figure 2. - Hole porosity variations in the 8- by 6-Foot Supersonic Wind Tunnel transonic test section.

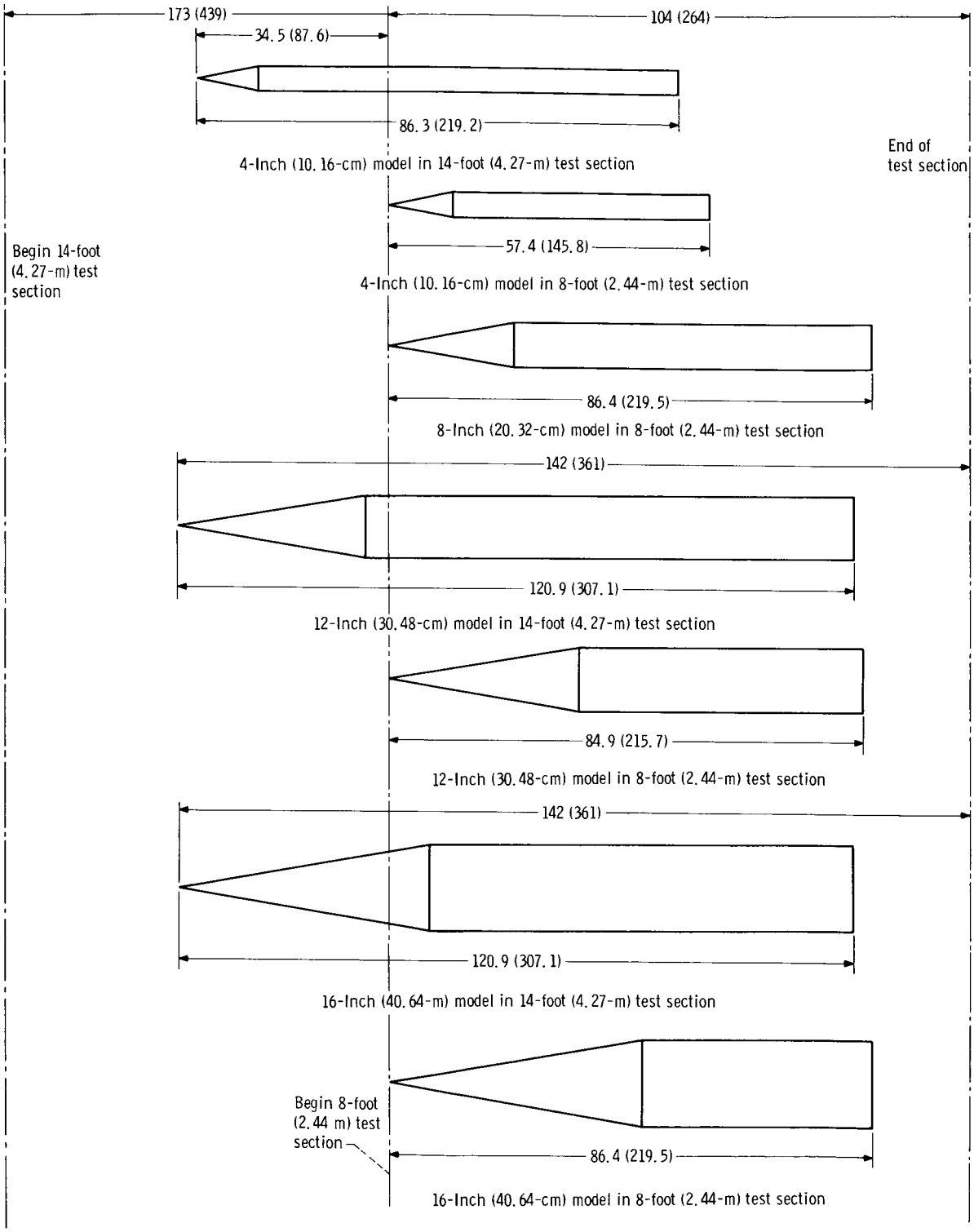

Figure 3. - Model dimensions and test locations. (Dimensions are in inches (cm).)

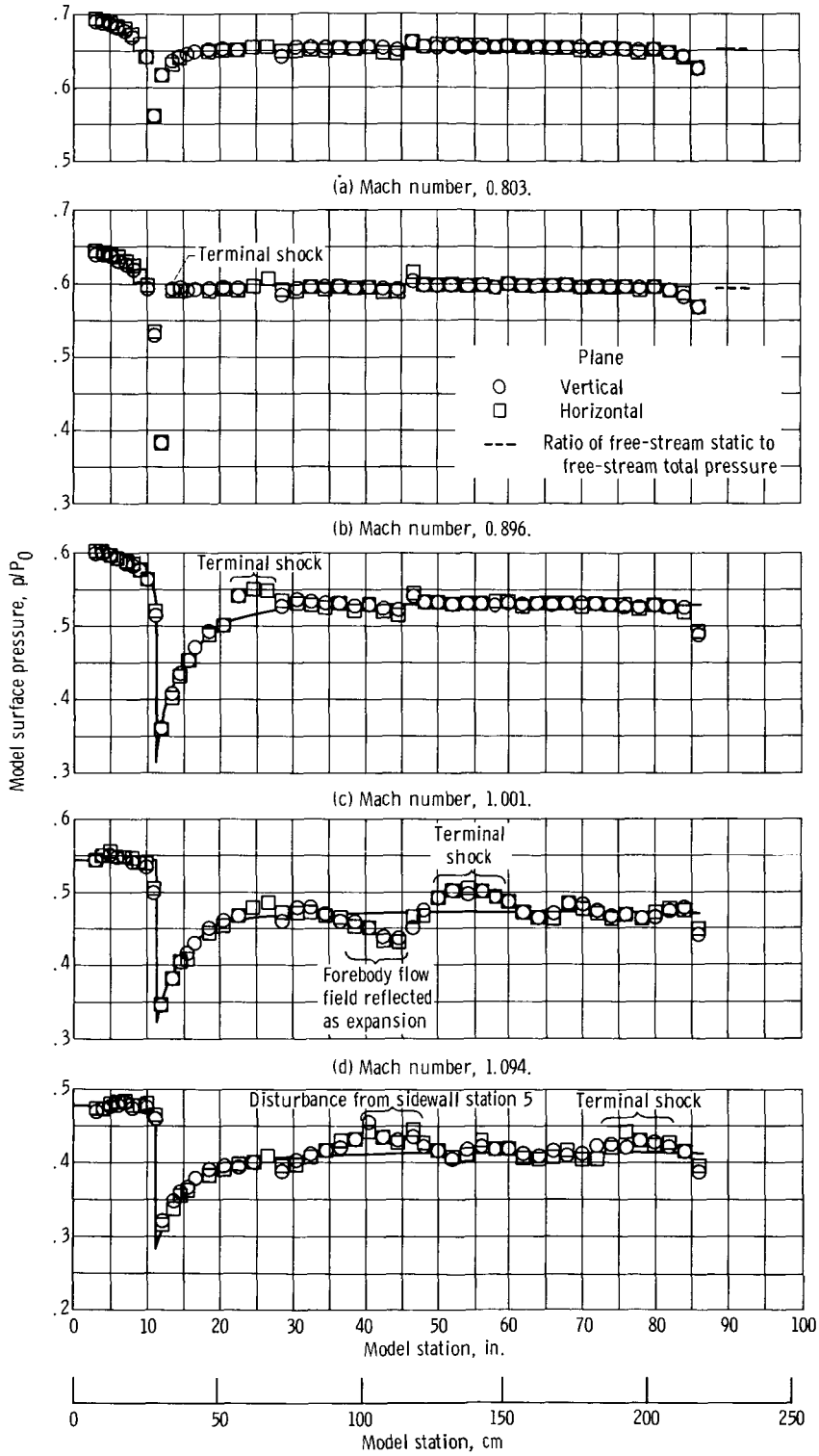

Figure 4. - Pressure distributions on 4-inch (10.16-cm) diameter 10° half-angle cone-cylinder model in 14-foot (4.27-m) - 5.8-percent porosity test section.

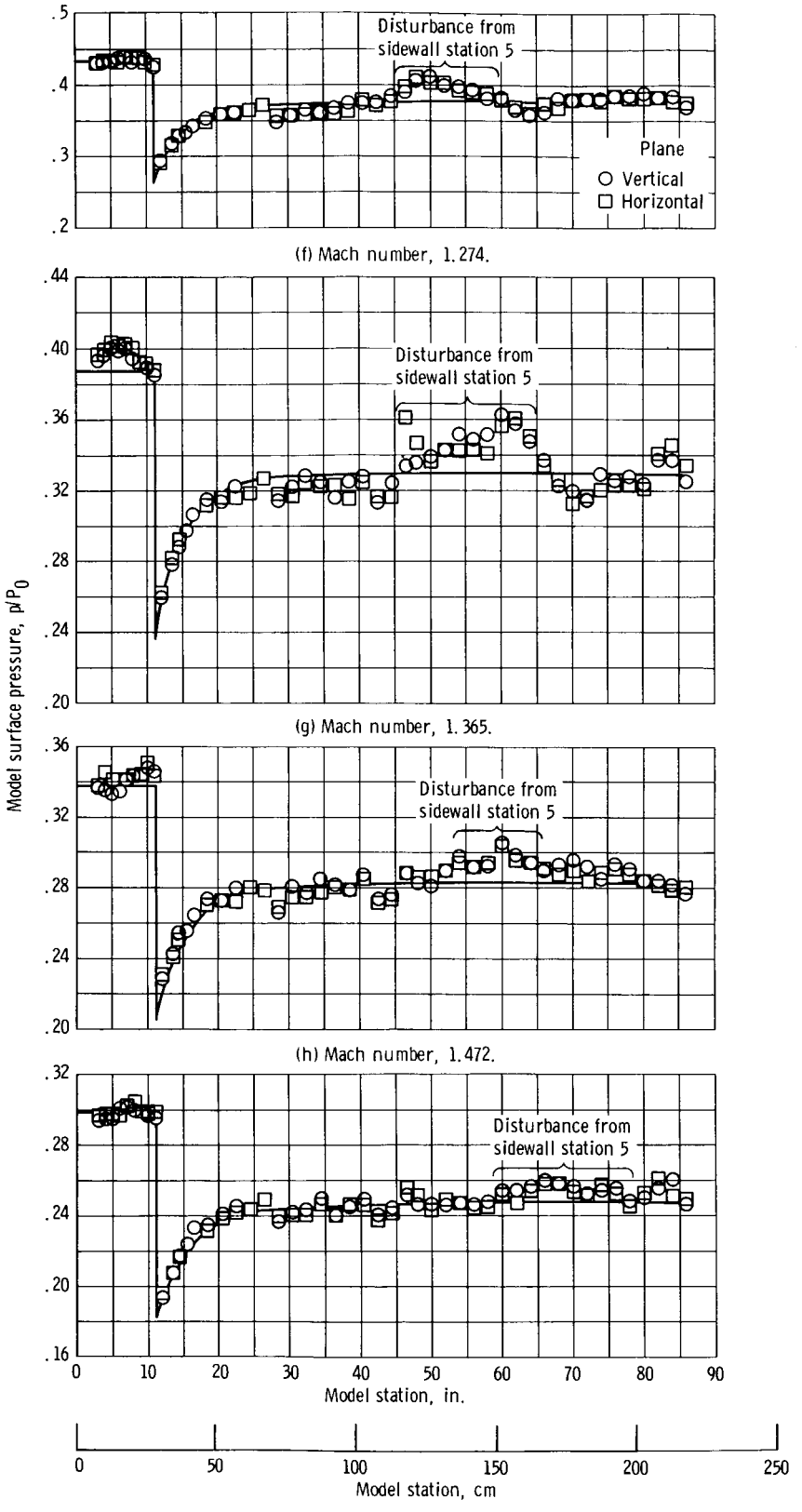

(f) Mach number, 1.274.

(g) Mach number, 1.365.

(h) Mach number, 1.472.

(i) Mach number, 1.564.

Figure 4. - Continued.

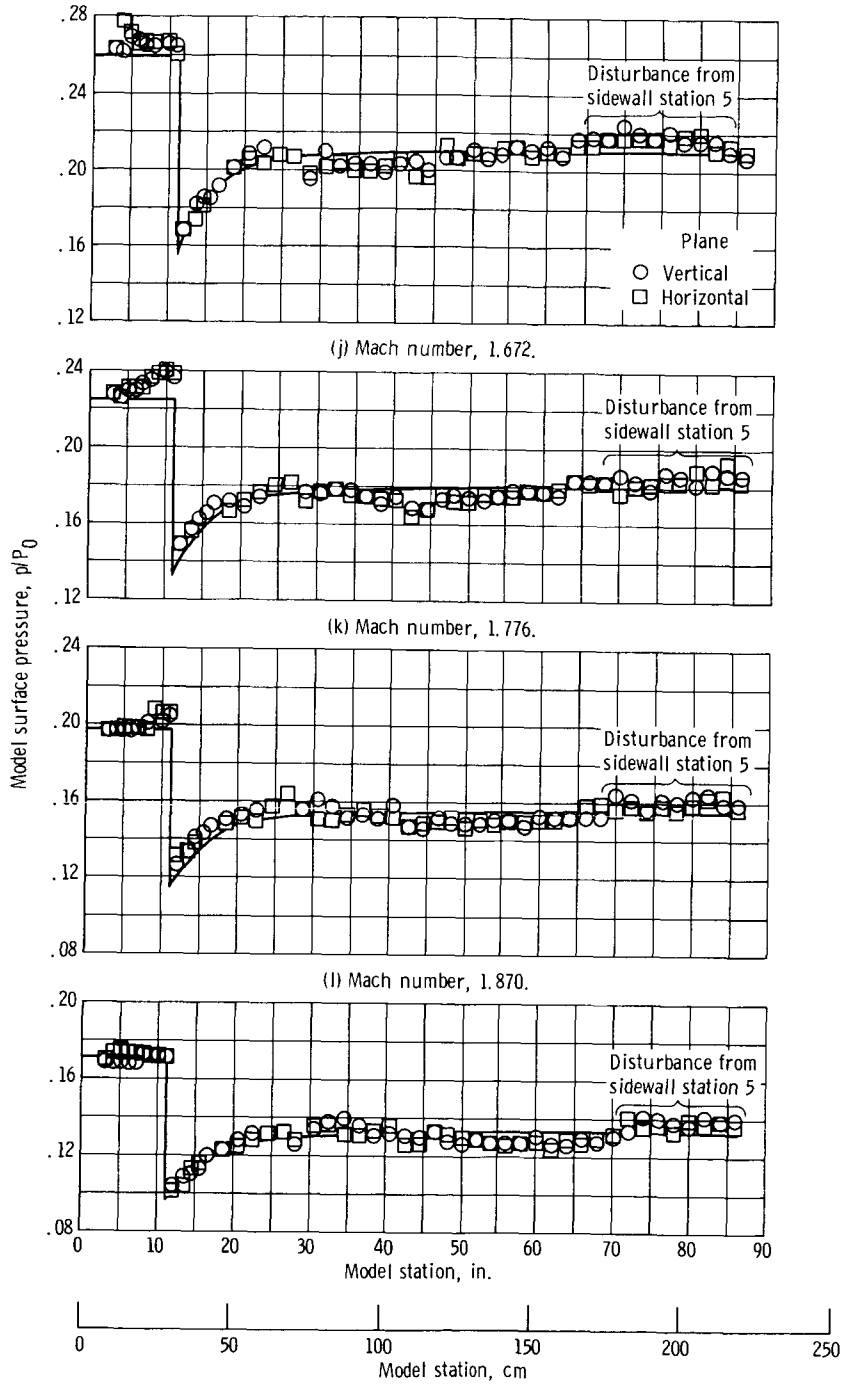

(j) Mach number, 1.672.

(k) Mach number, 1.776.

(l) Mach number, 1.870.

(m) Mach number, 1.974.

Figure 4. - Concluded.

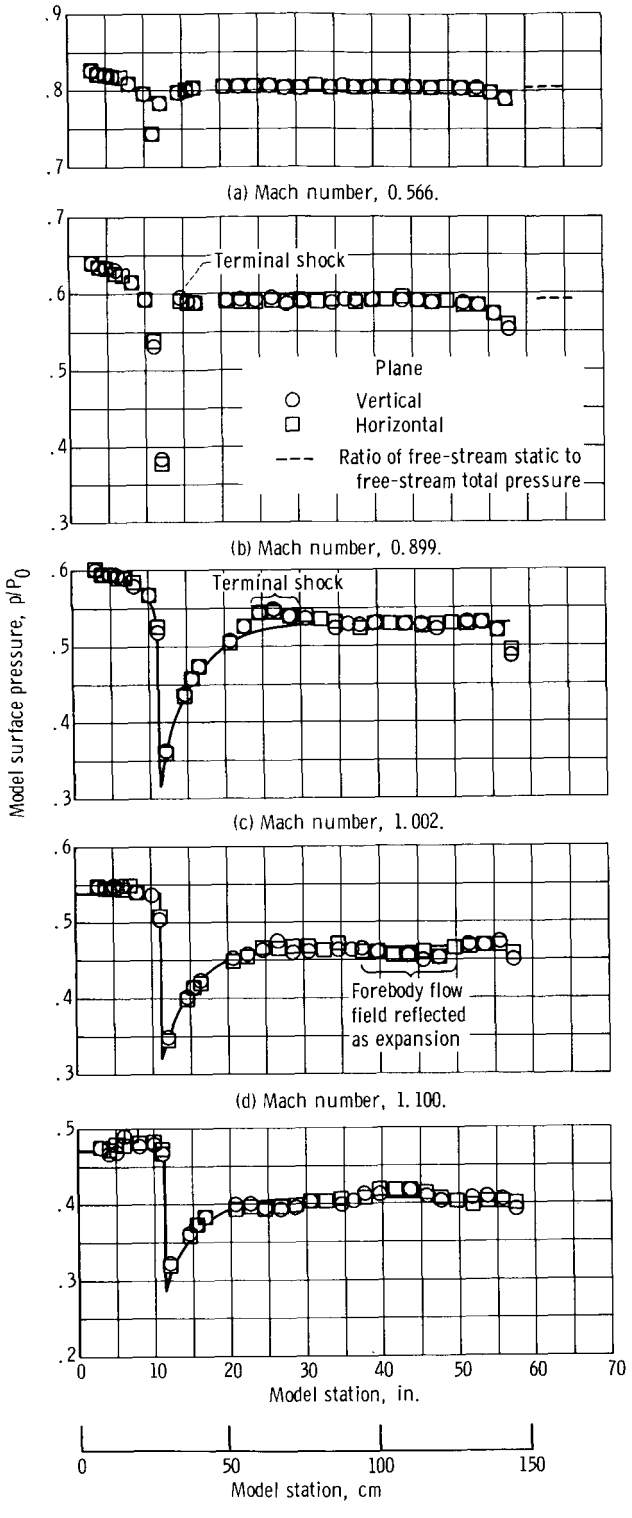

Figure 5. - Pressure distributions on 4-inch (10.16-cm) diameter 10° half-angle cone-cylinder model in 8-foot (2.44-m) - 3.1-percent porosity test section.

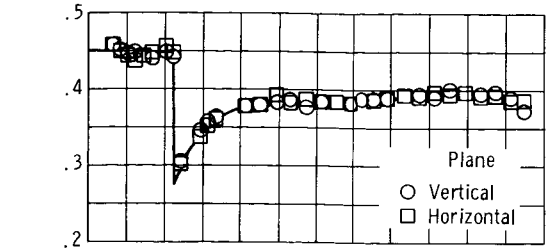

(f) Mach number, 1.242.

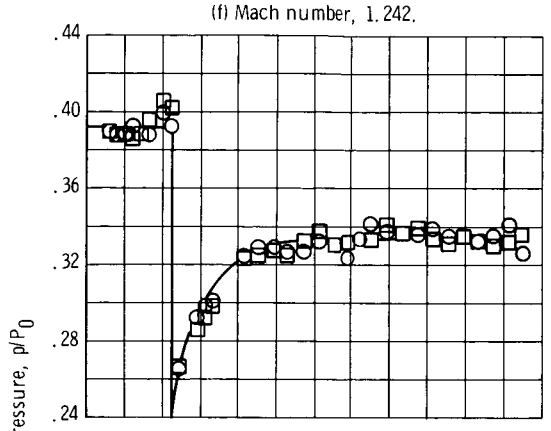

(g) Mach number, 1.356.

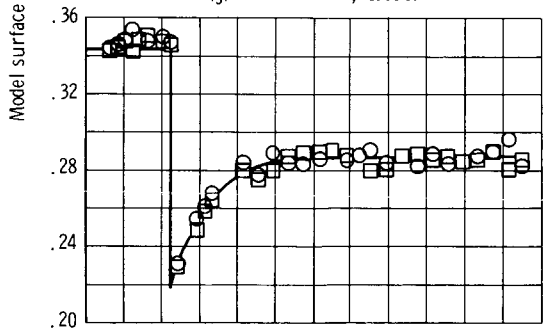

(h) Mach number, 1.461.

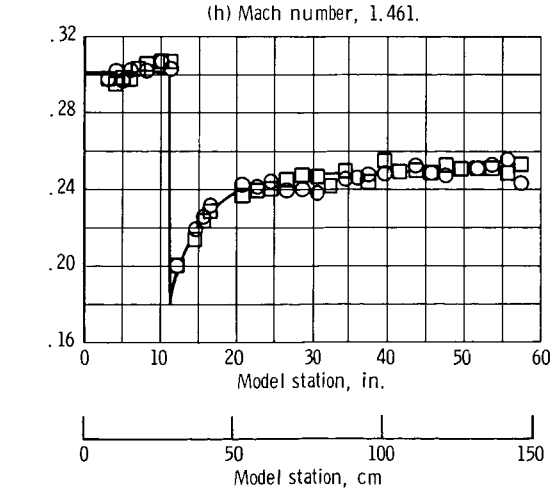

Model surface pressure, p/P_0

(i) Mach number, 1.558.

Figure 5. - Continued.

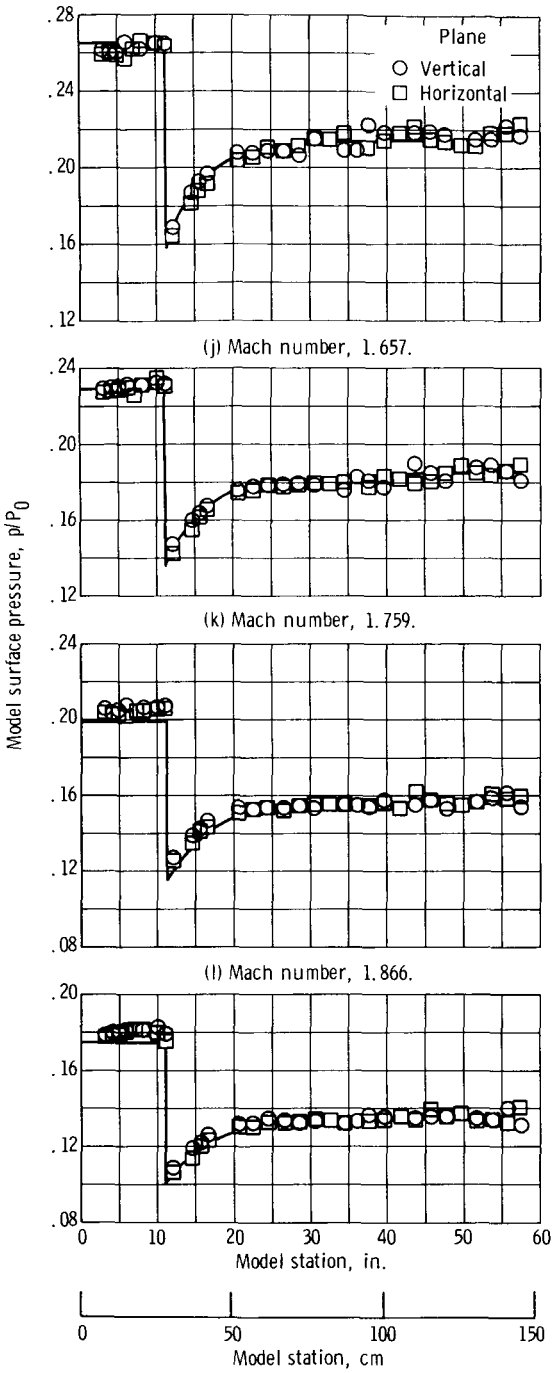

(j) Mach number, 1.657.

(k) Mach number, 1.759.

(l) Mach number, 1.866.

(m) Mach number, 1.958.

Figure 5. - Concluded.

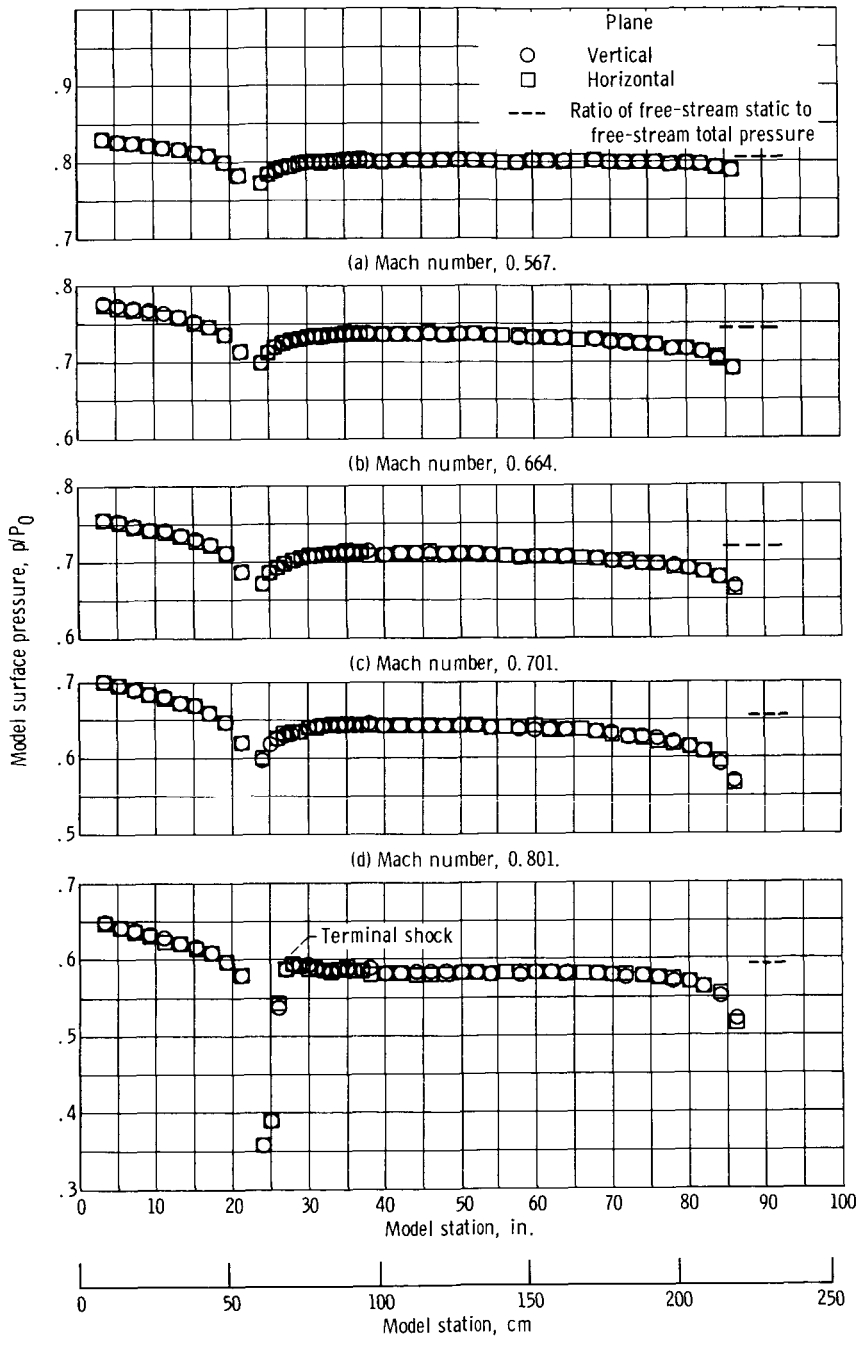

Figure 6. - Pressure distributions on 8-inch (20.32-cm) diameter 10° half-angle cone-cylinder model in 8-foot (2.44-cm) - 6.2-percent porosity test section.

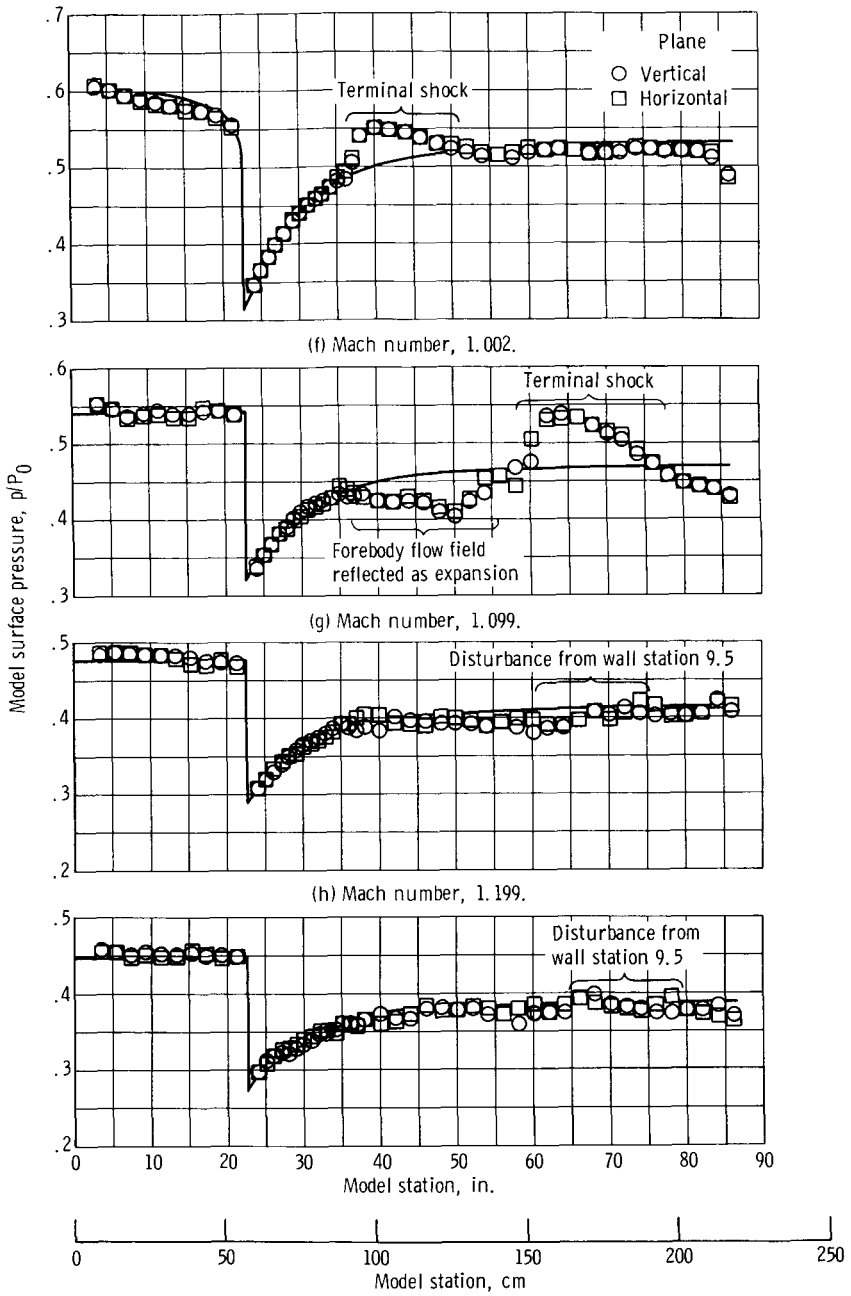

(f) Mach number, 1.002.

(g) Mach number, 1.099.

(h) Mach number, 1.199.

(i) Mach number, 1.248.

Figure 6. - Continued.

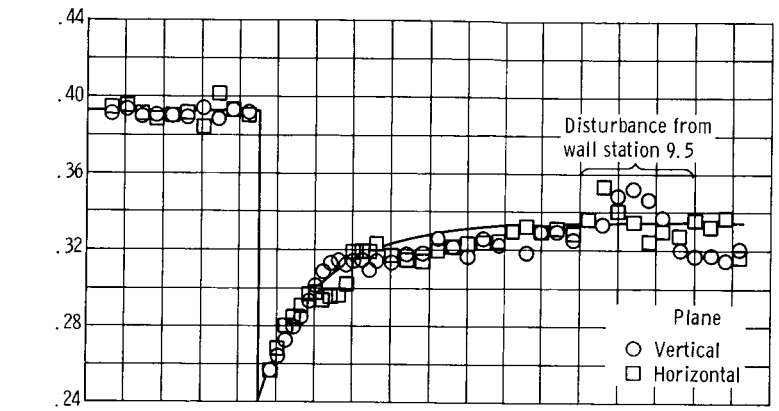

(j) Mach number, 1.355.

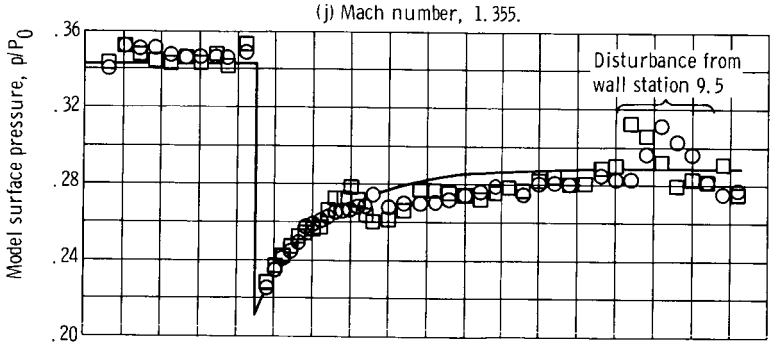

(k) Mach number, 1.459.

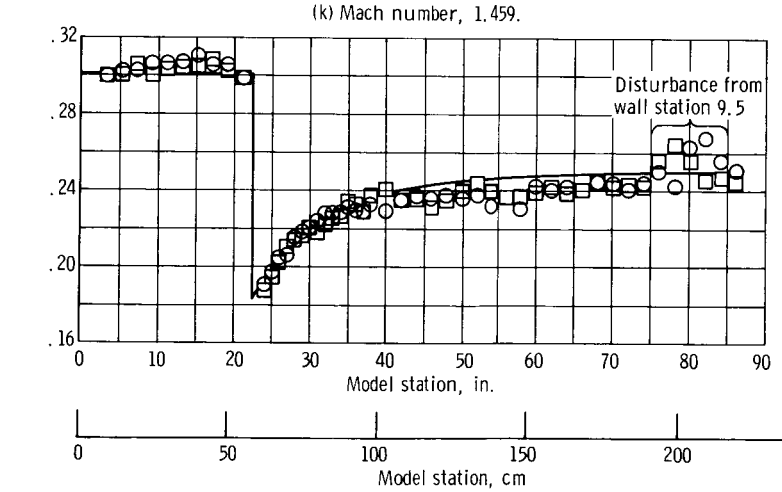

(l) Mach number, 1.559.

Figure 6. - Continued.

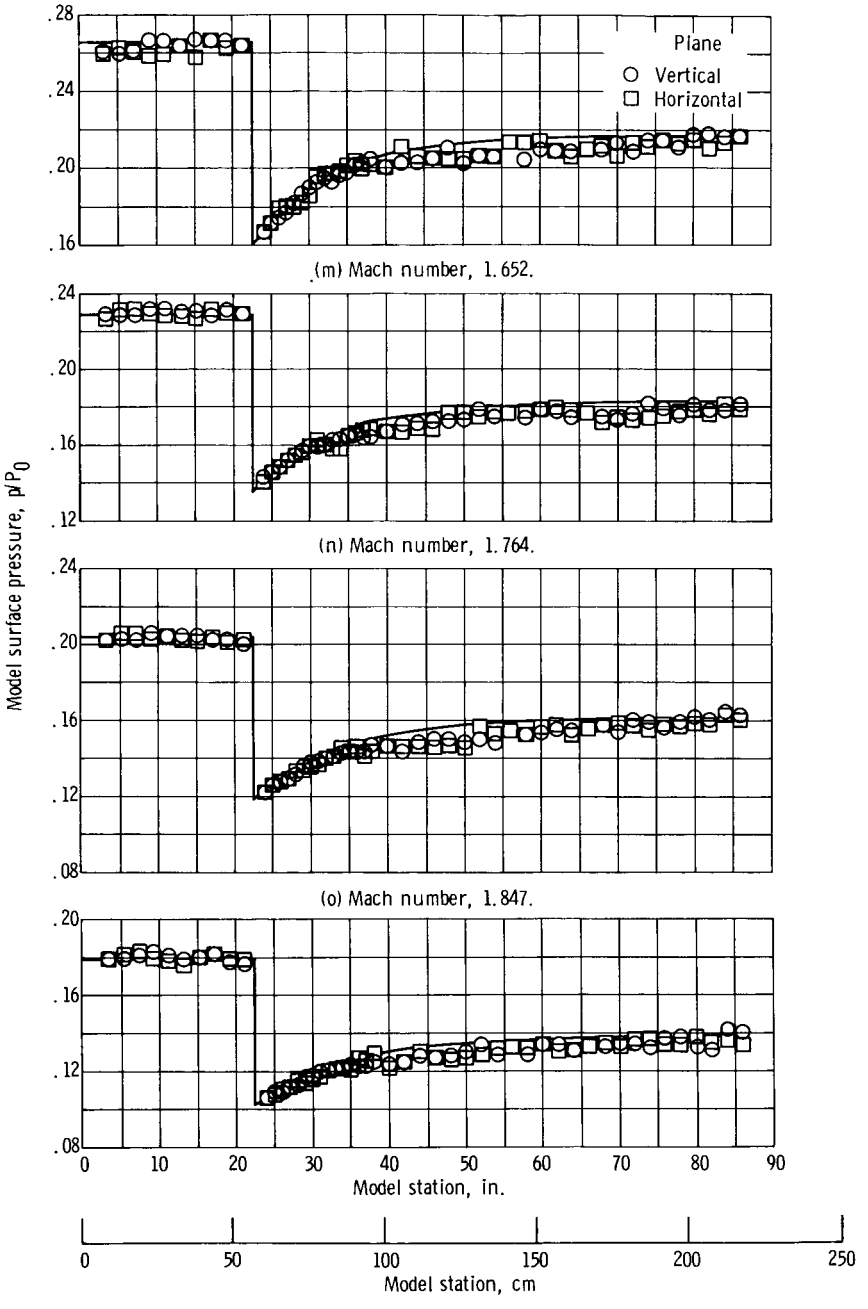

Figure 6. - Concluded.

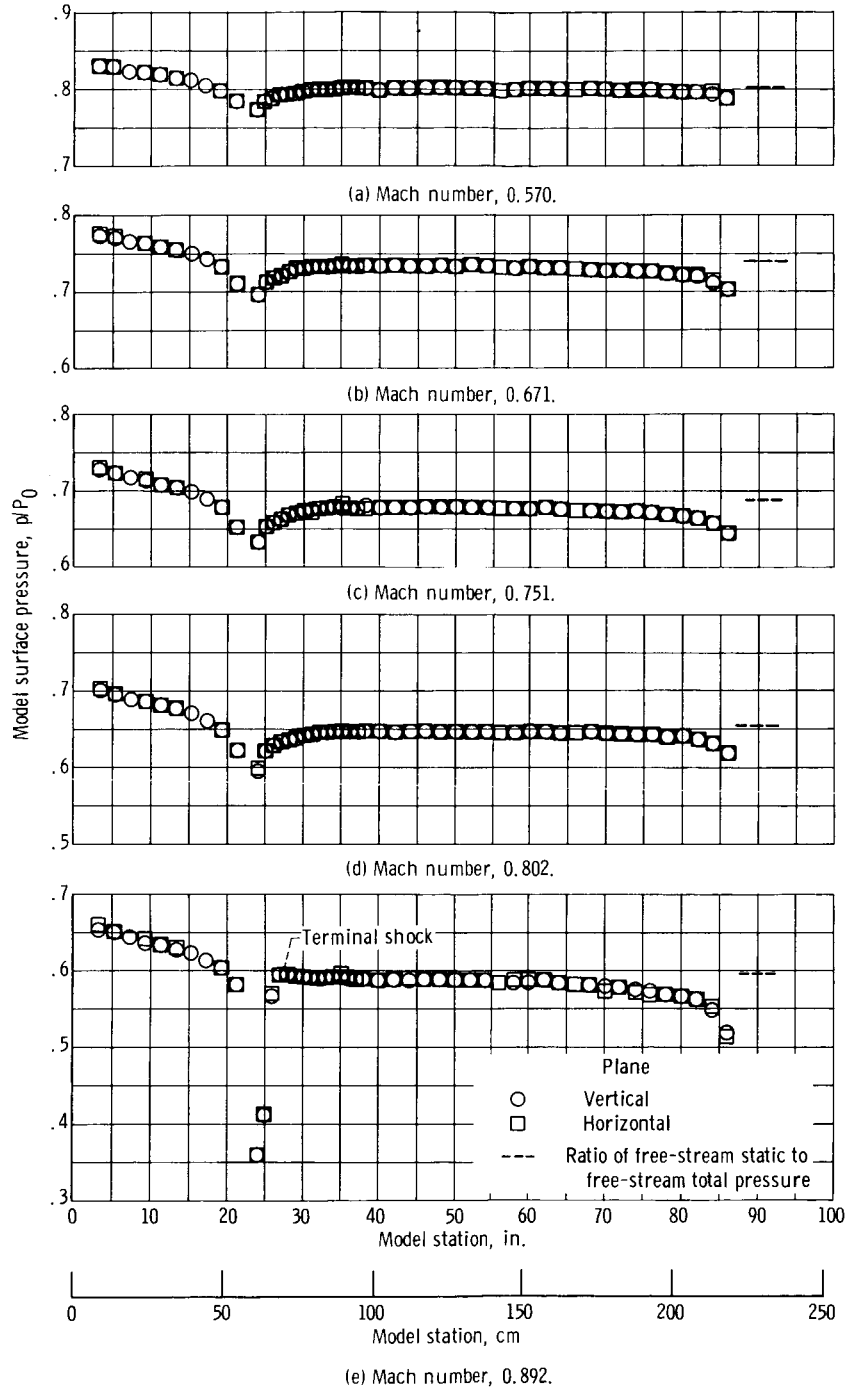

Figure 7. - Pressure distributions on 8-inch (20.32-cm) diameter 10° half-angle cone-cylinder model in 8-foot (2.44-m) - 3.1-percent porosity test section.

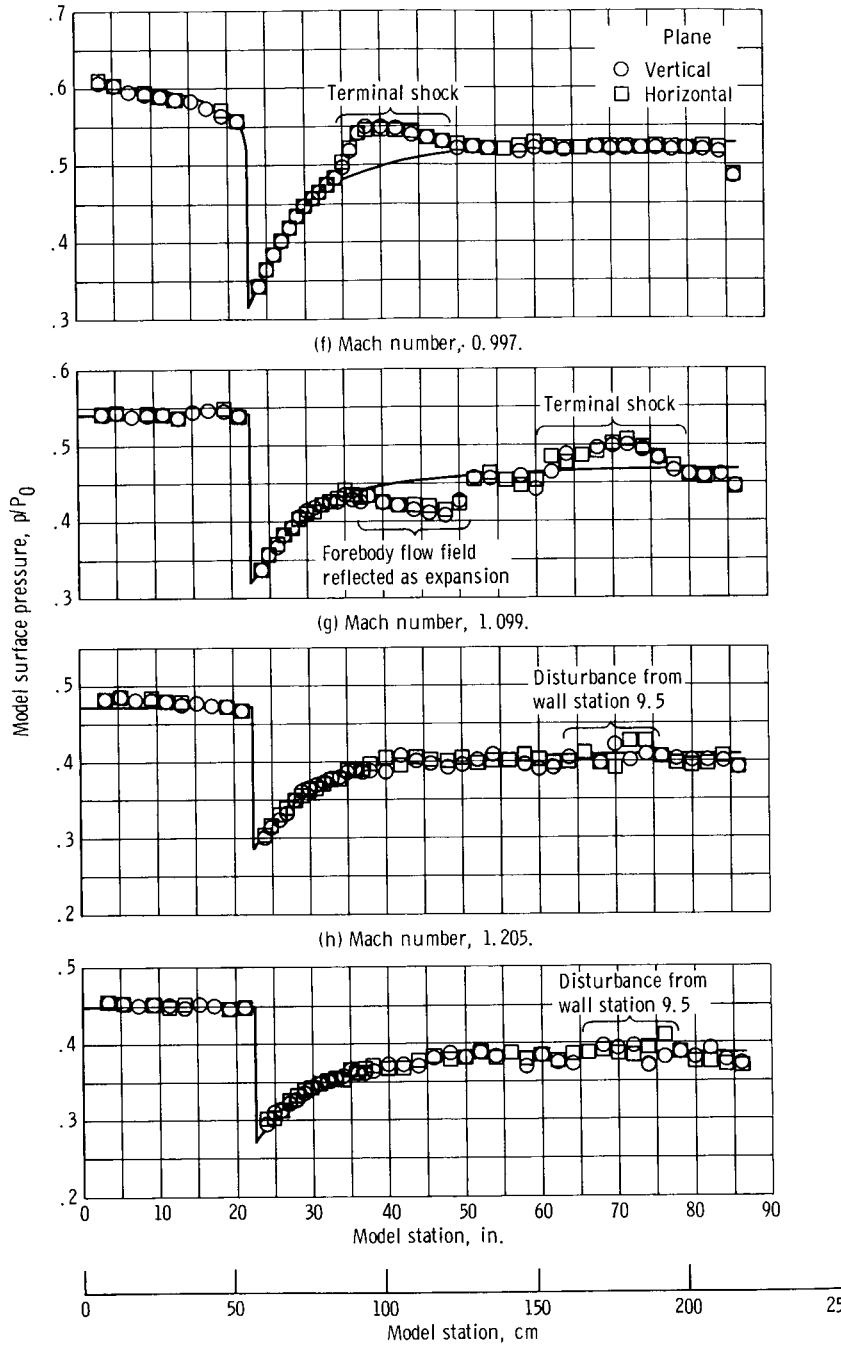

(f) Mach number, 0.997.

(g) Mach number, 1.099.

(h) Mach number, 1.205.

(i) Mach number, 1.247.

Figure 7. - Continued.

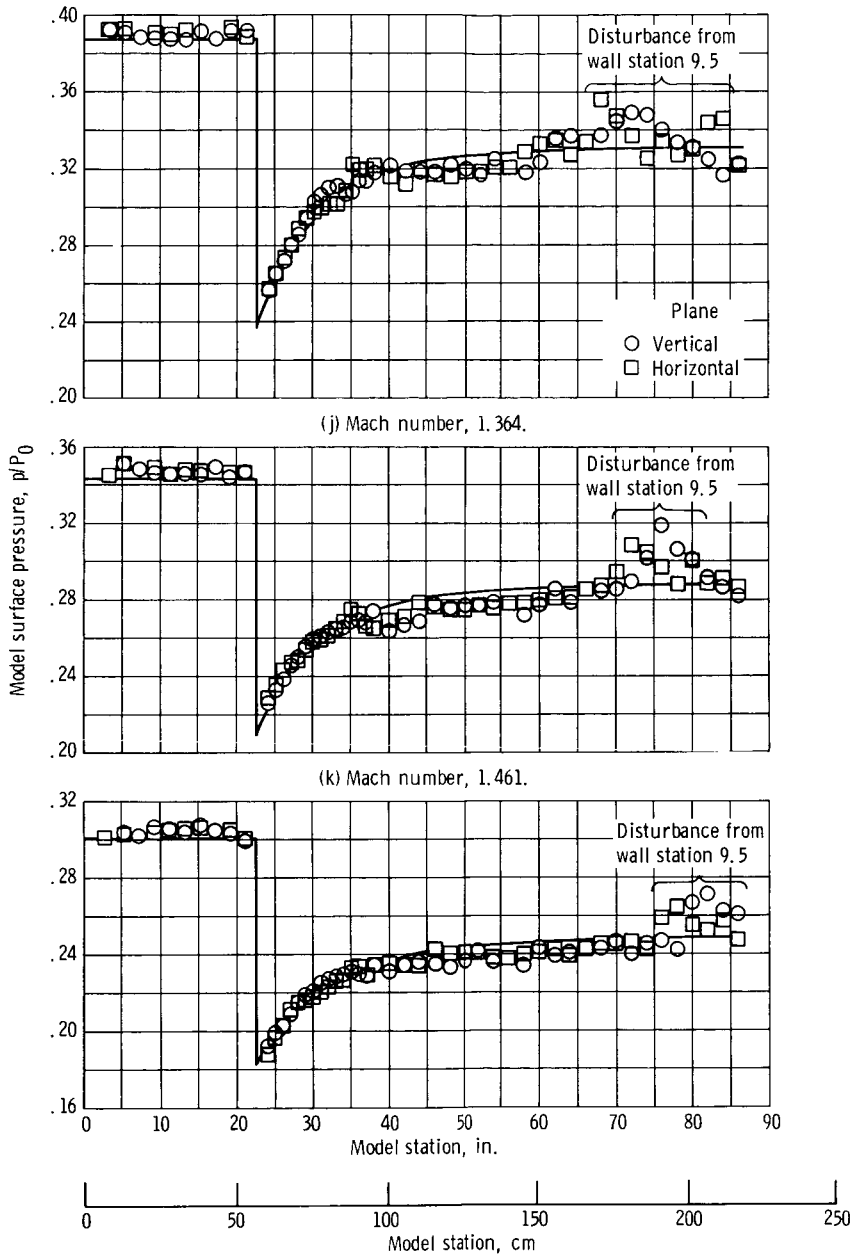

(j) Mach number, 1.364.

(k) Mach number, 1.461.

(l) Mach number, 1.561.

Figure 7. - Continued.

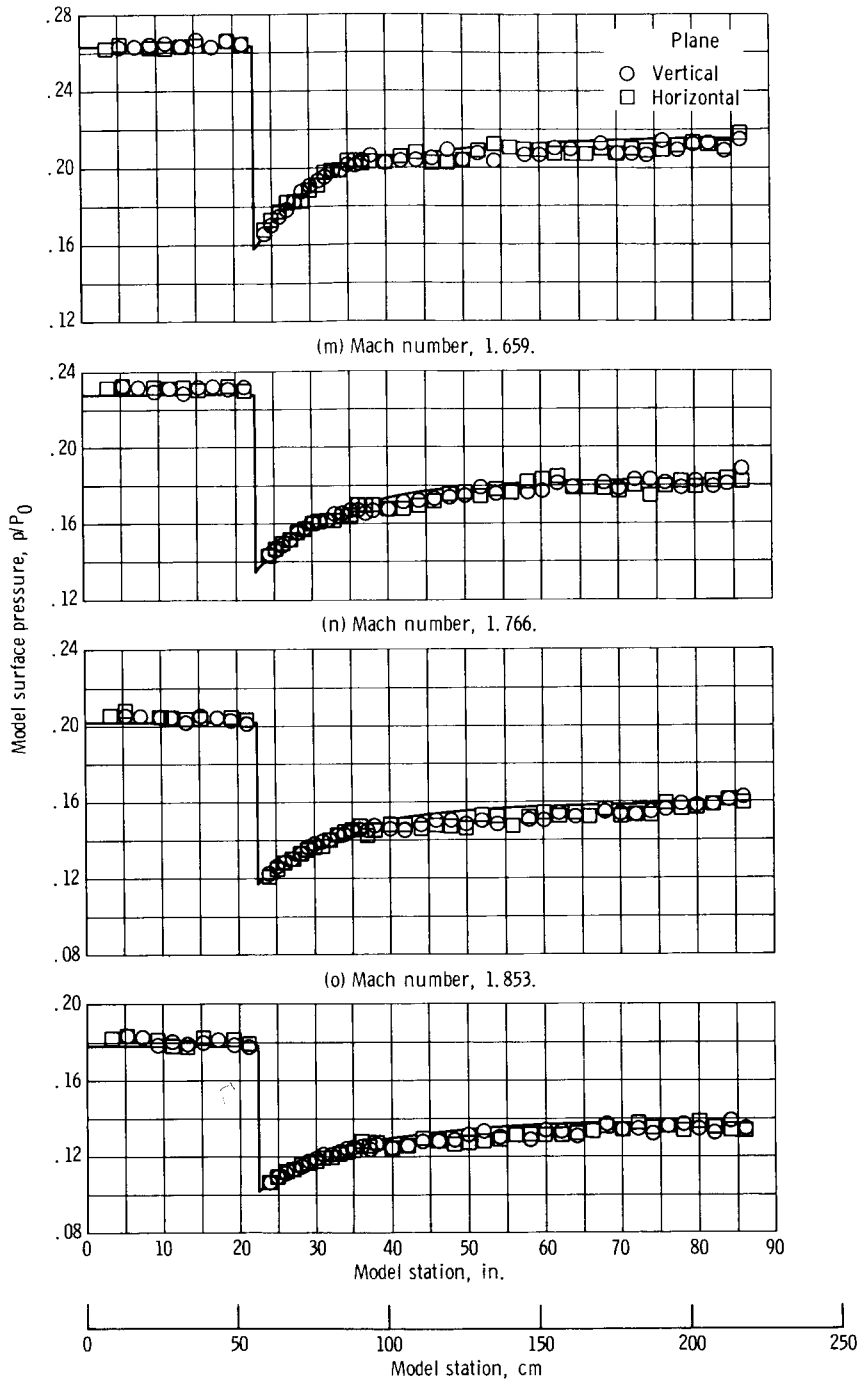

Figure 7. - Concluded.

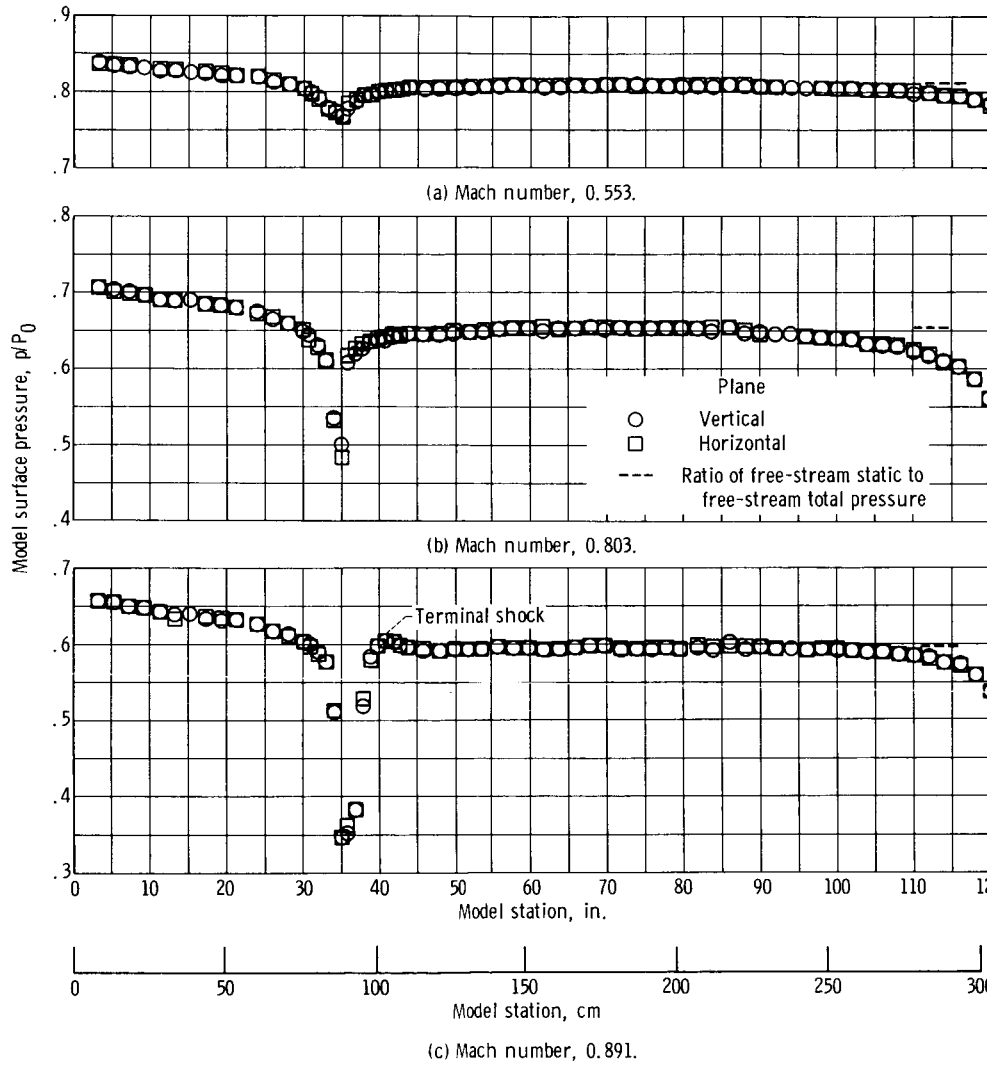

Figure 8. - Pressure distributions on 12-inch (30.48-cm) diameter 10° half-angle cone-cylinder model in 14-foot (4.27-m) - 5.8-percent porosity test section.

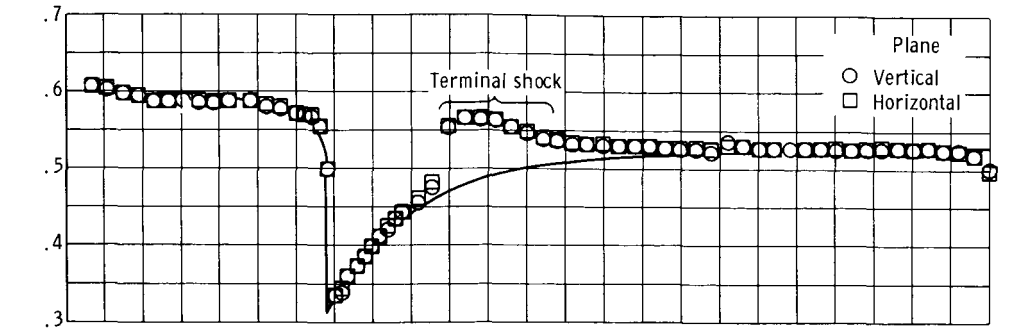

(d) Mach number, 1.003.

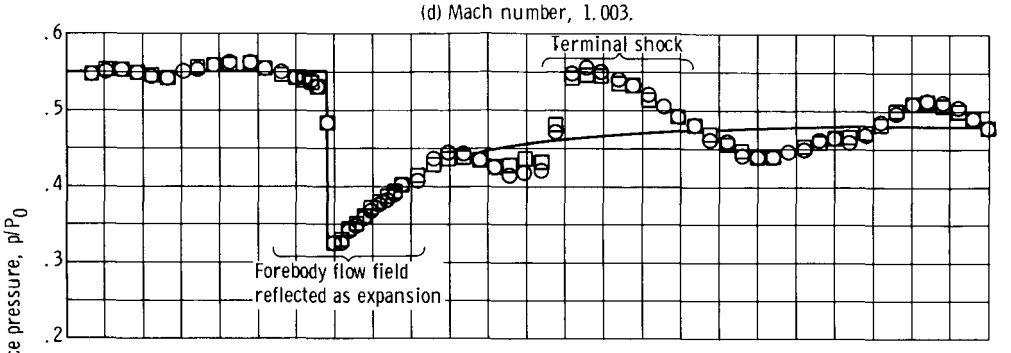

(e) Mach number, 1.084.

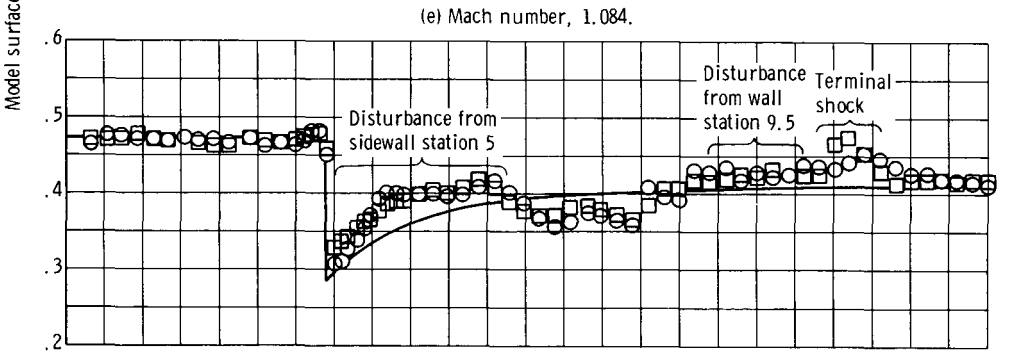

(f) Mach number, 1.206.

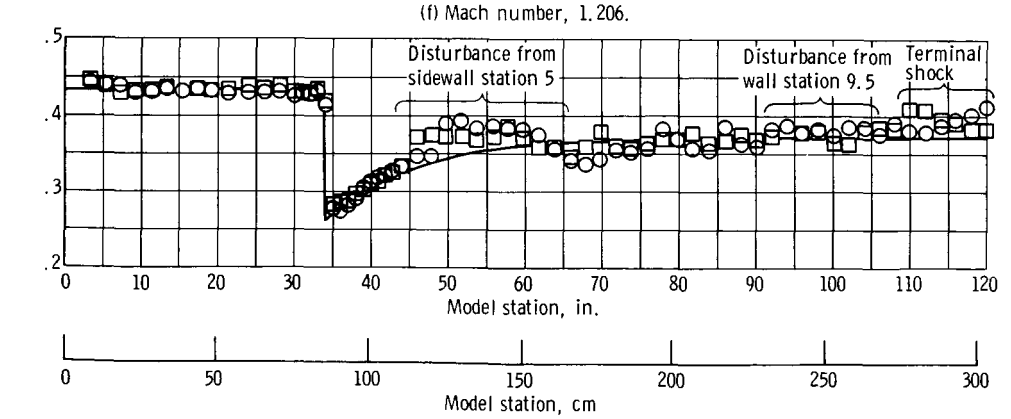

(g) Mach number, 1.275.

Figure 8. - Continued.

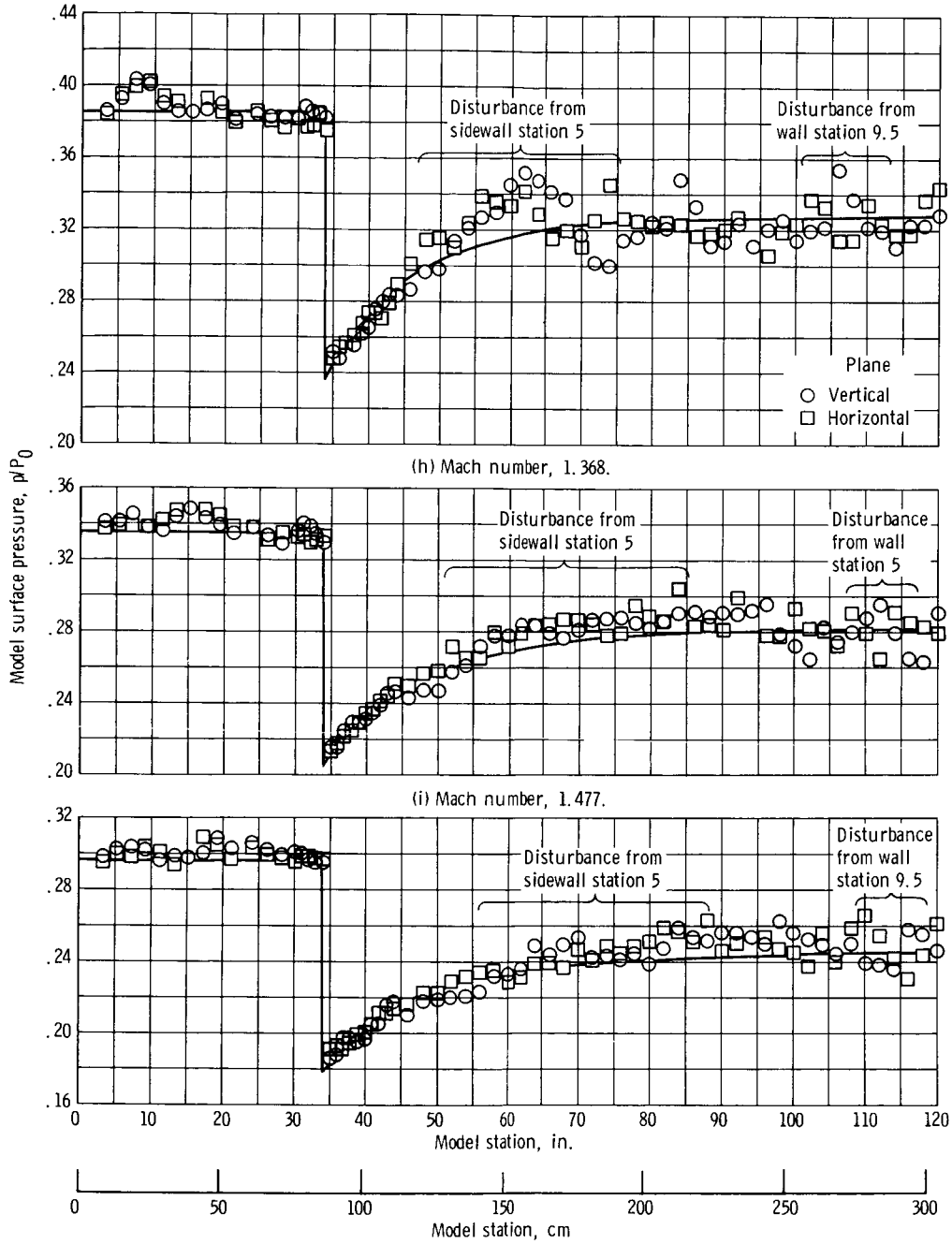

Figure 8. - Continued.

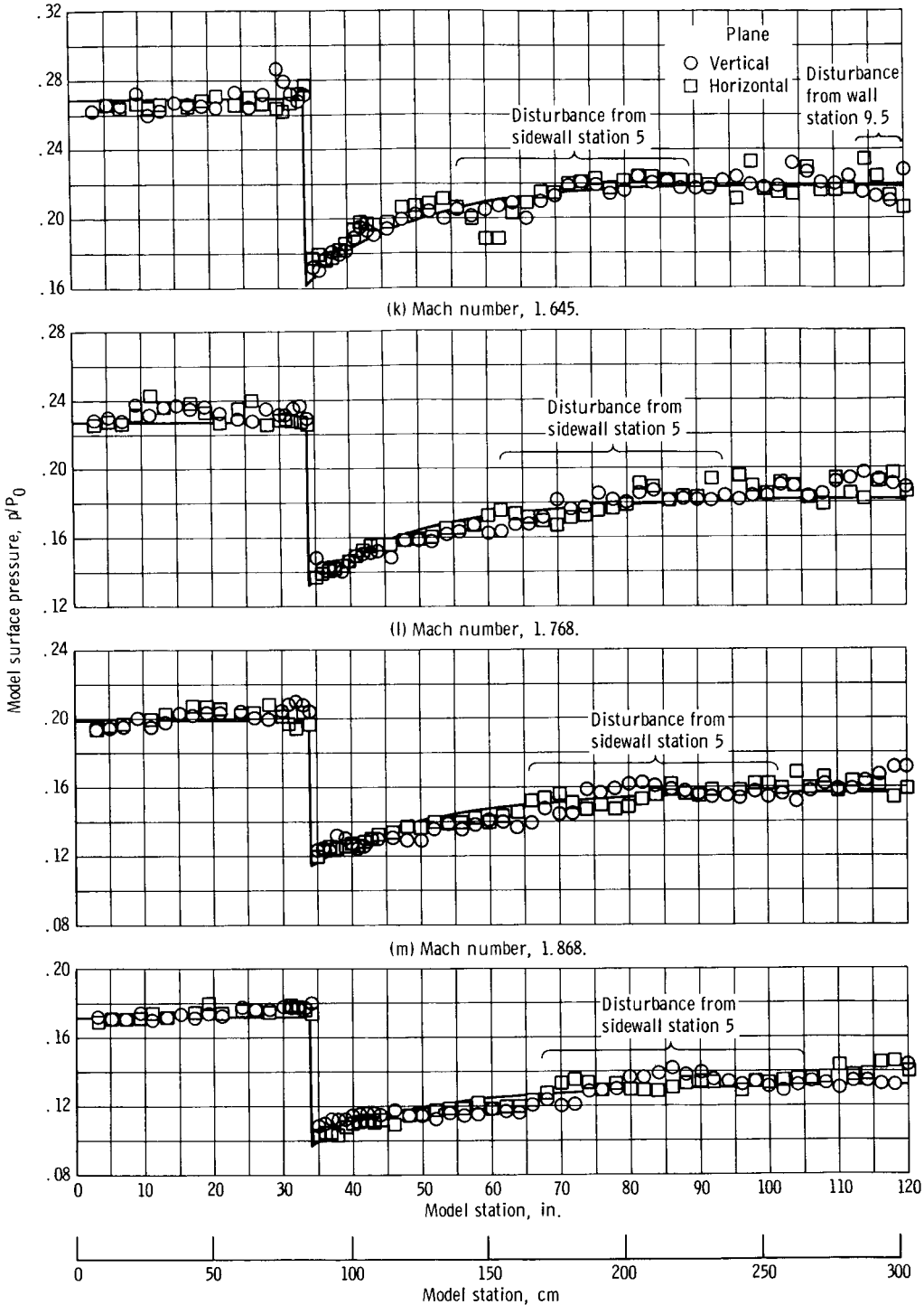

(k) Mach number, 1.645.

(l) Mach number, 1.768.

(m) Mach number, 1.868.

(n) Mach number, 1.972.

Figure 8. - Concluded.

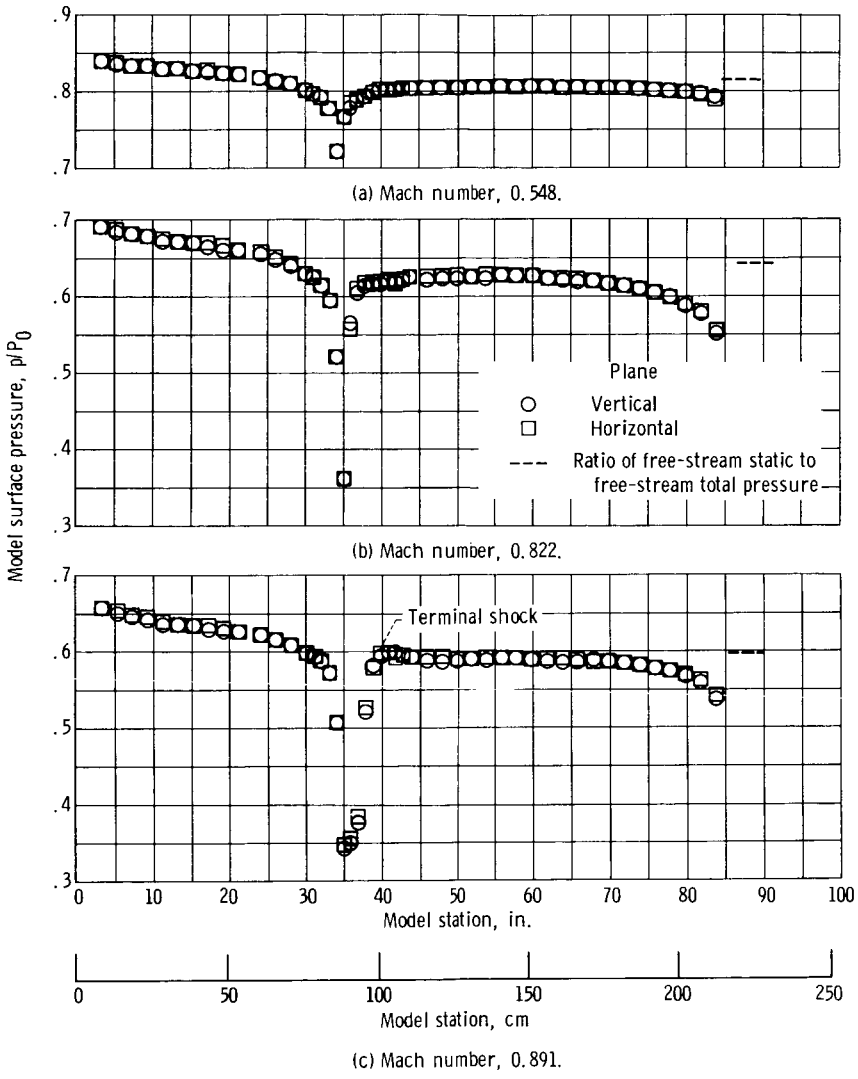

Figure 9. - Pressure distributions on 12-inch (30.48-cm) diameter 10° half-angle cone-cylinder model in 8-foot (2.44-cm) - 6.2-percent porosity test section.

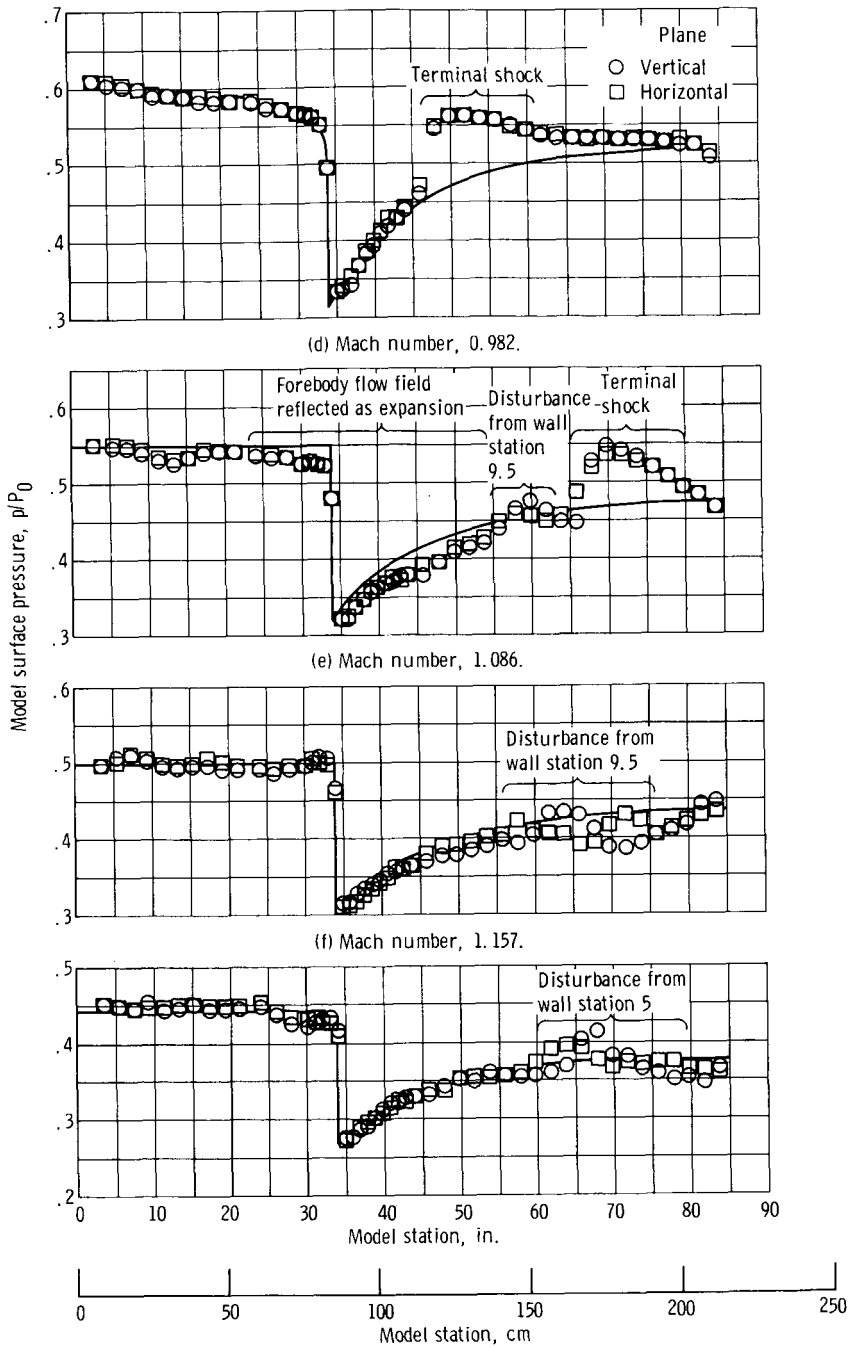

(d) Mach number, 0.982.

(e) Mach number, 1.086.

(f) Mach number, 1.157.

(g) Mach number, 1.259.

Figure 9. - Continued.

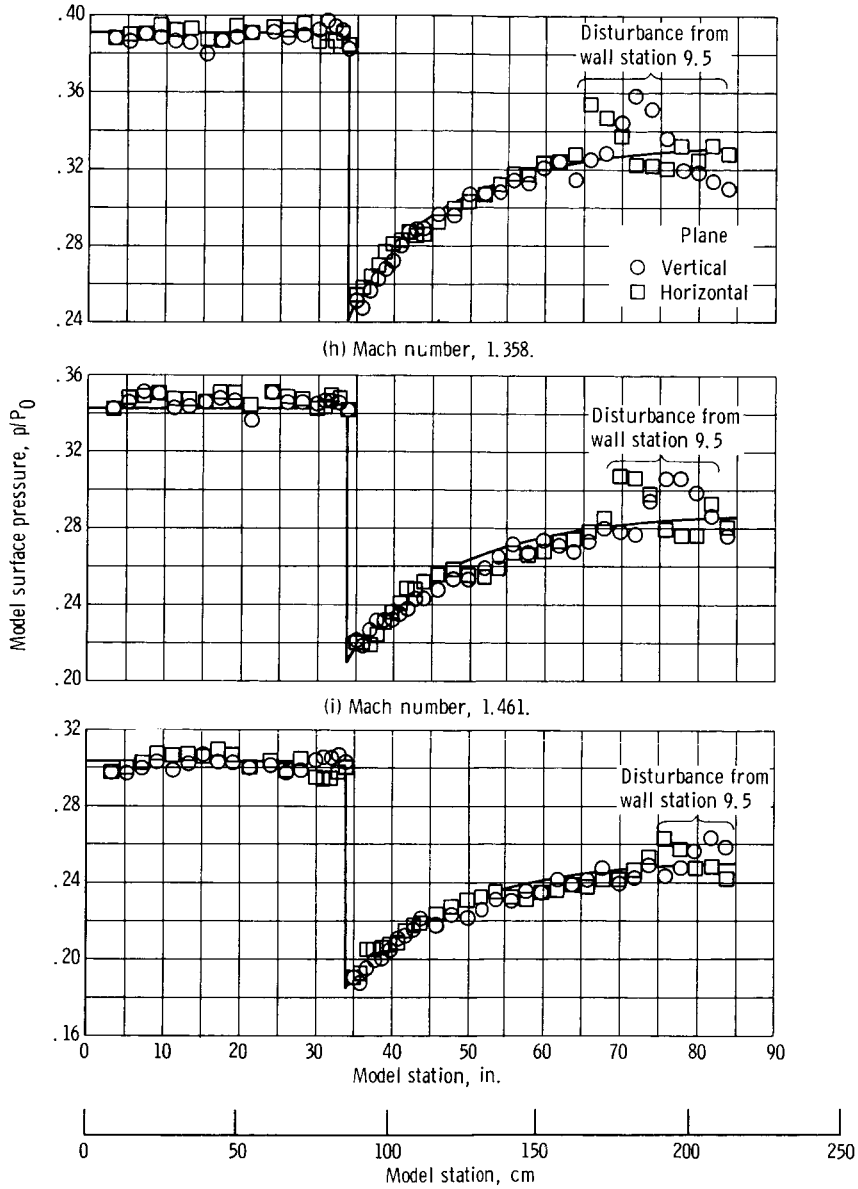

(h) Mach number, 1.358.

(i) Mach number, 1.461.

(j) Mach number, 1.552.

Figure 9. - Continued.

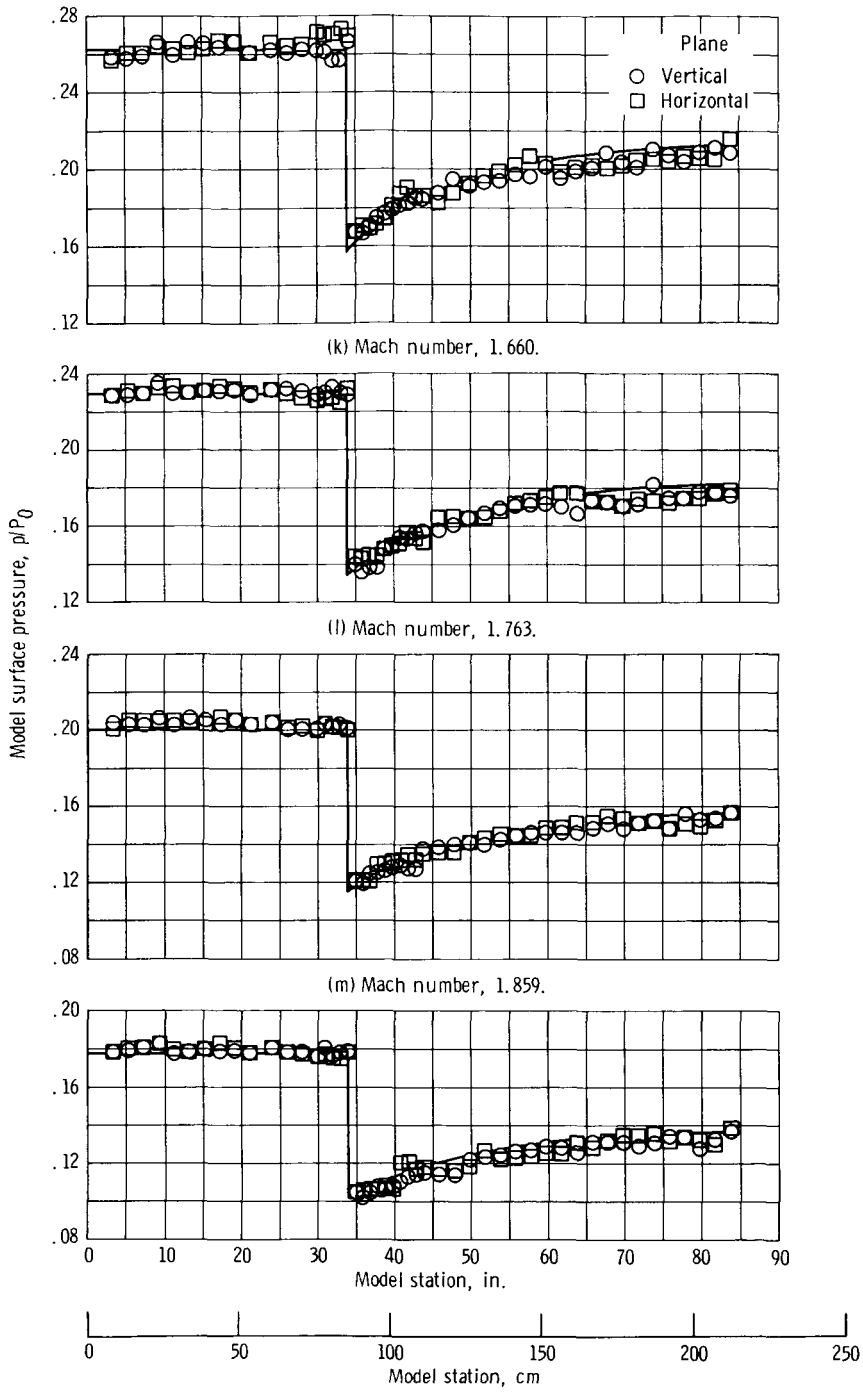

(k) Mach number, 1.660.

(l) Mach number, 1.763.

(m) Mach number, 1.859.

(n) Mach number, 1.945.

Figure 9. - Concluded.

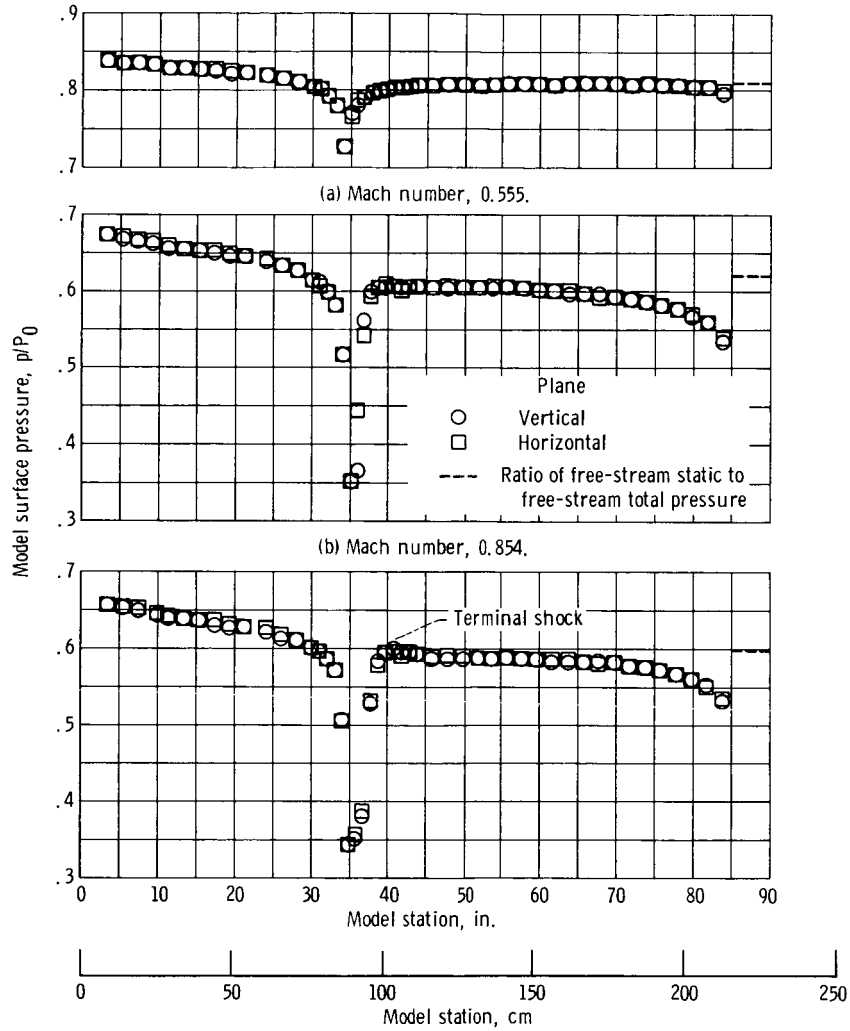

Figure 10. - Pressure distuributions on 12-inch (30.48-cm) diameter 10° half-angle cone-cylinder model in 8-foot (2.44-m) - 3.1-percent porosity test section.

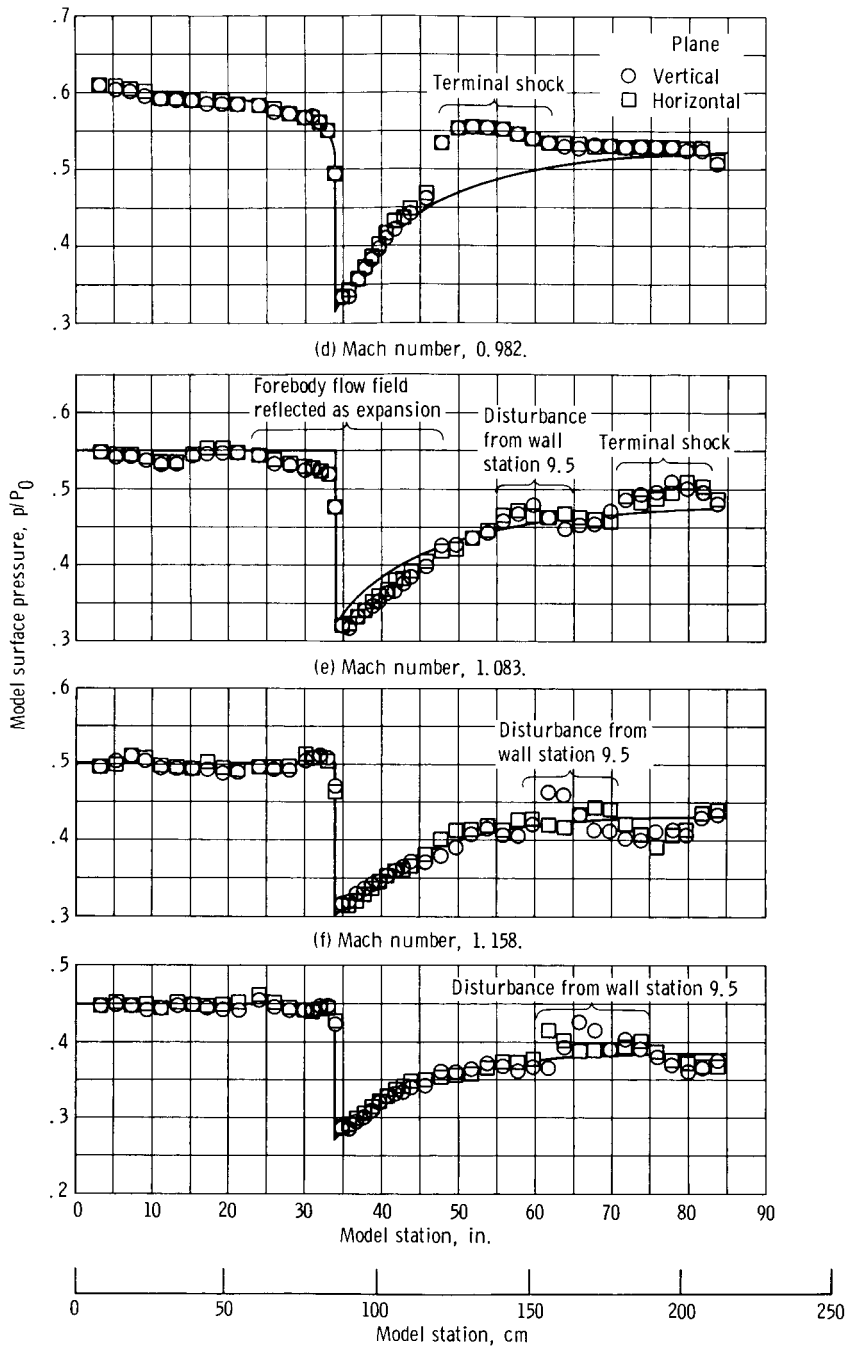

(d) Mach number, 0.982.

(e) Mach number, 1.083.

(f) Mach number, 1.158.

(g) Mach number, 1.246.

Figure 10. - Continued.

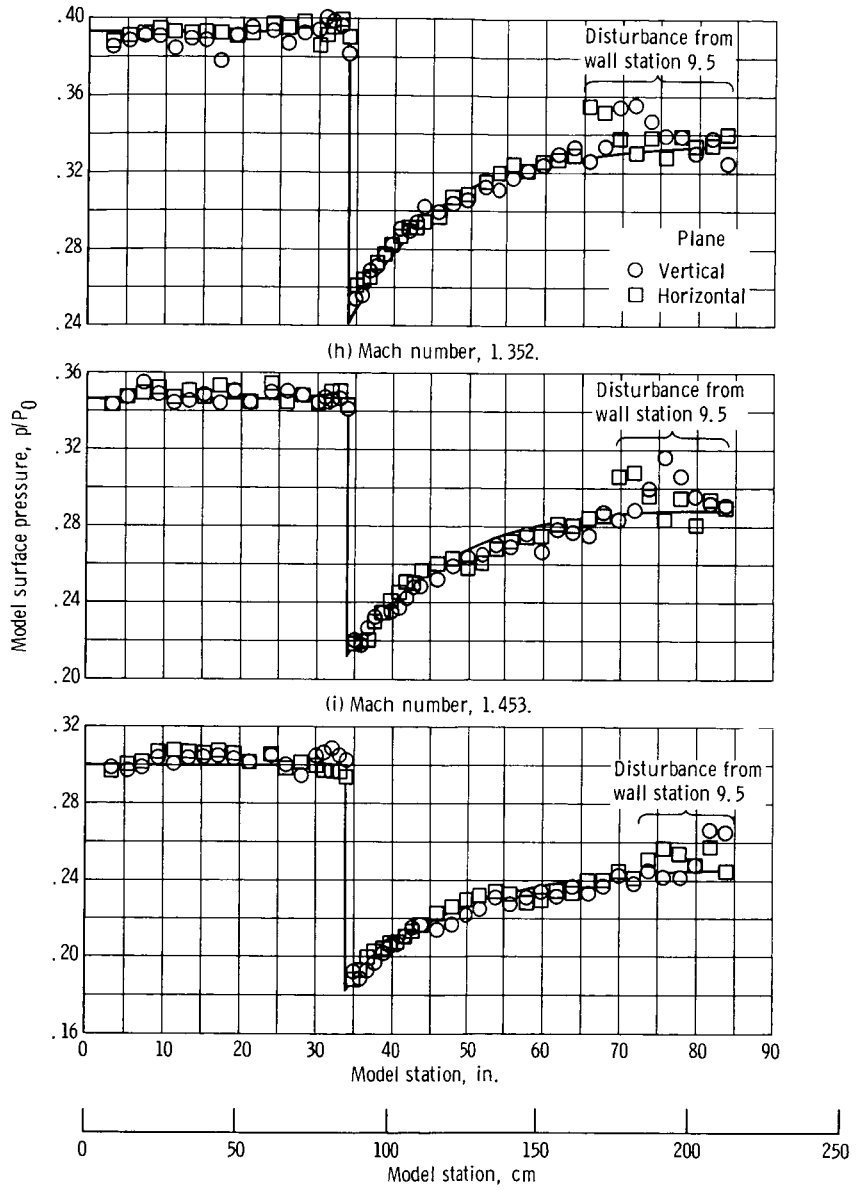

(h) Mach number, 1.352.

(i) Mach number, 1.453.

(j) Mach number, 1.562.

Figure 10. - Continued.

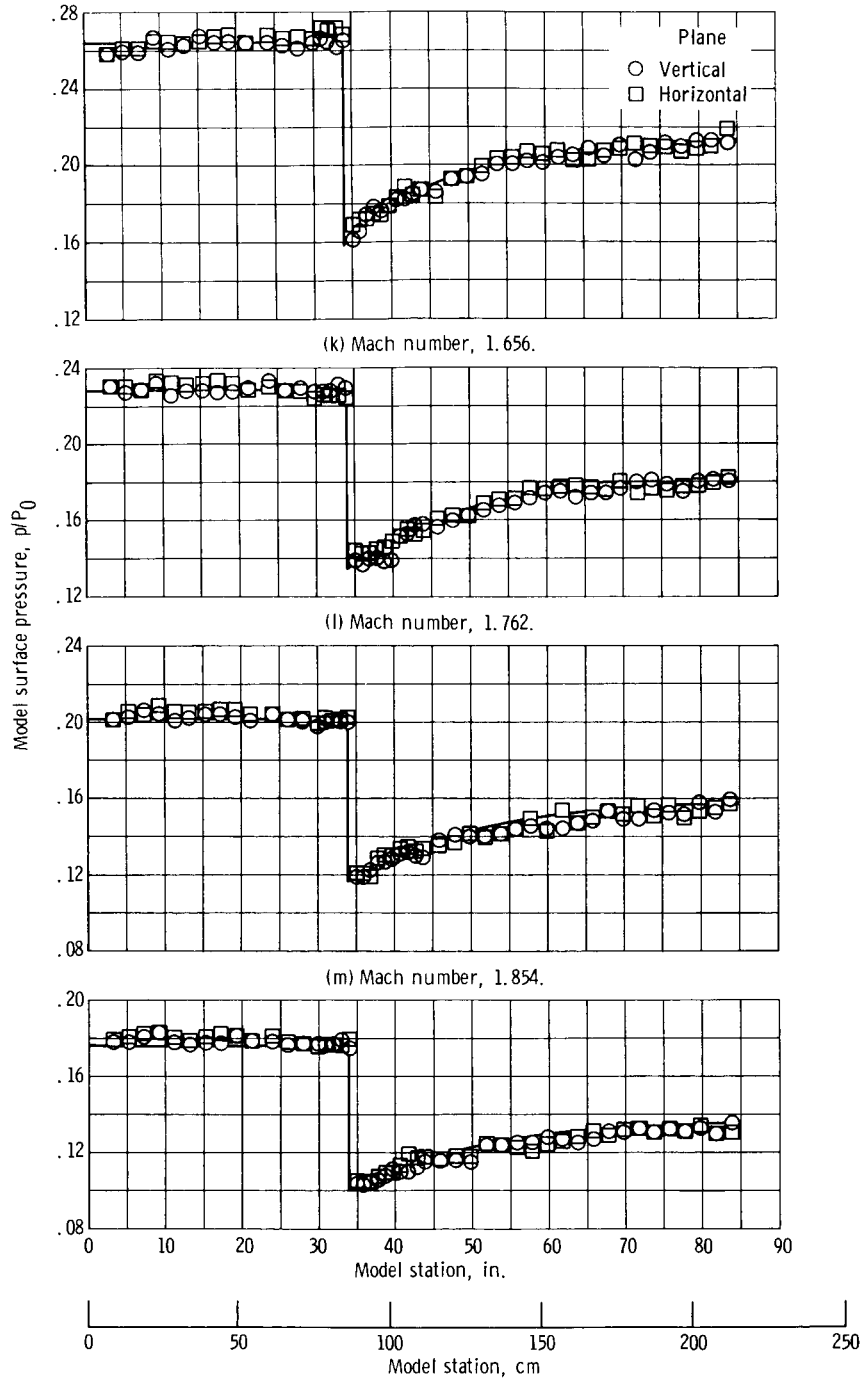

(k) Mach number, 1.656.

(l) Mach number, 1.762.

(m) Mach number, 1.854.

(n) Mach number, 1.950.

Figure 10. - Concluded.

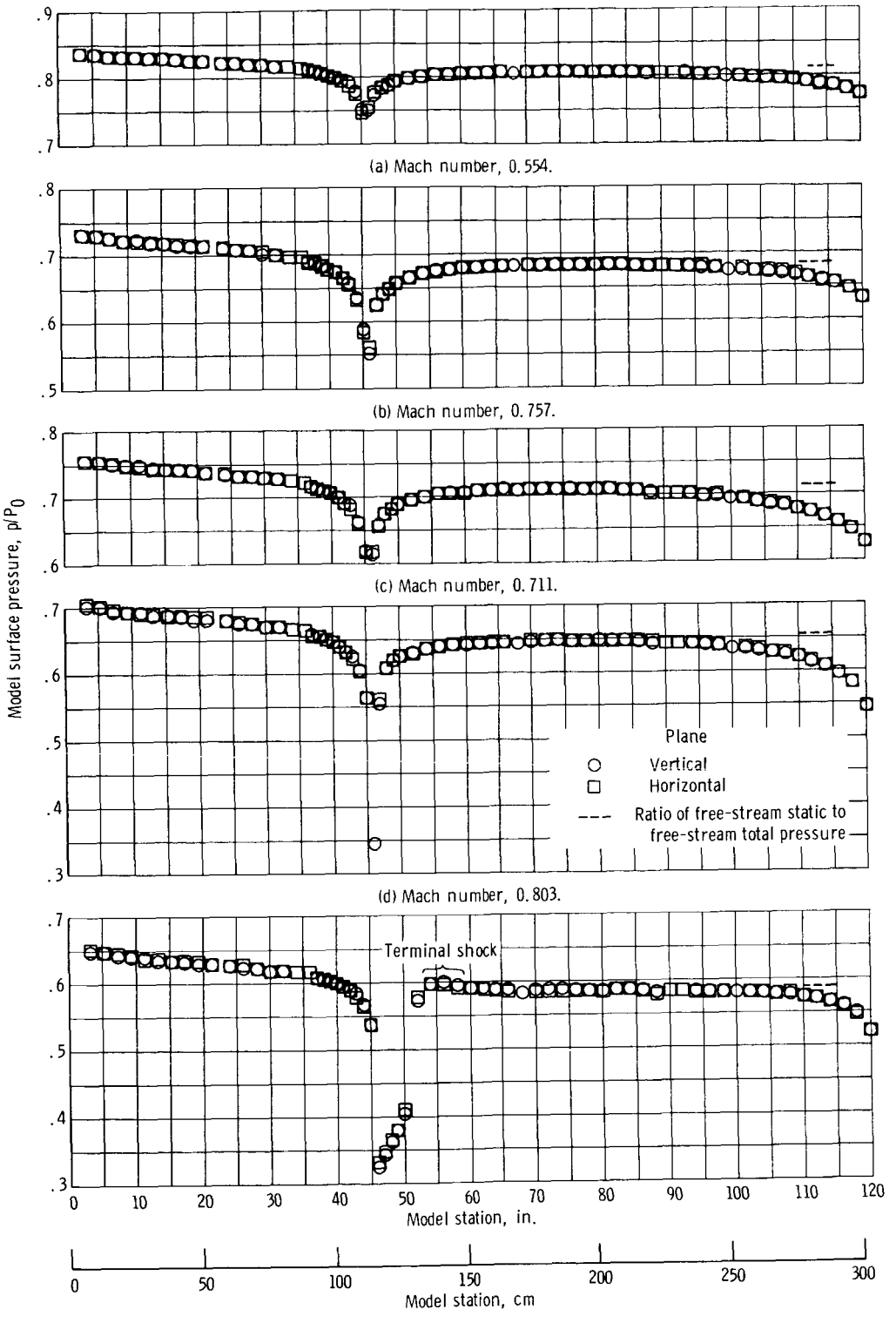

Figure 11. - Pressure distributions on 16-inch (40.64-cm) diameter 10° half-angle cone-cylinder model in 14-foot (4.27-m) - 5.8-percent porosity test section.

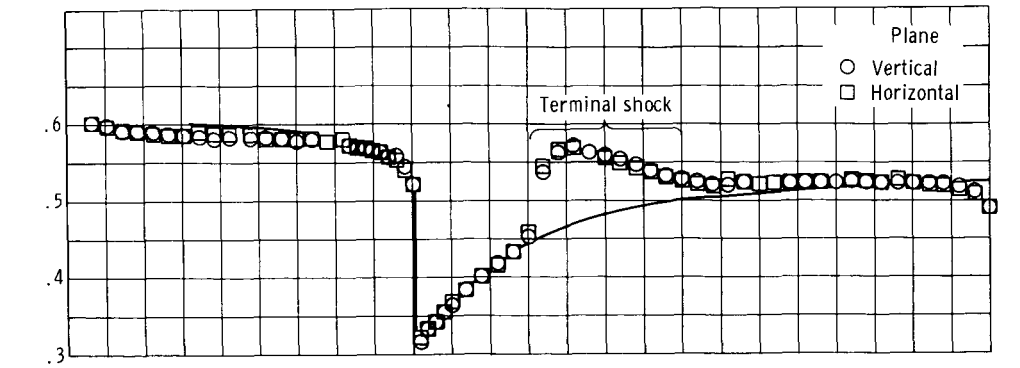

(f) Mach number, 1.002.

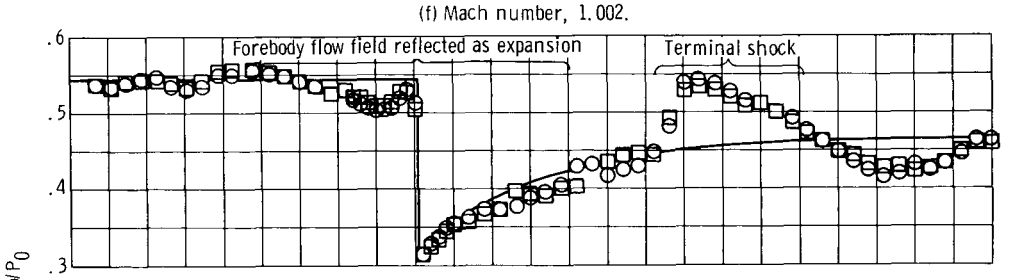

(g) Mach number, 1.096.

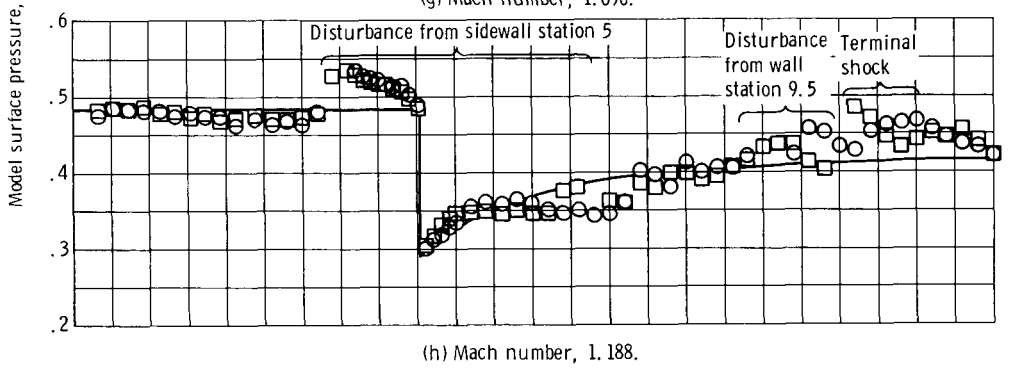

(h) Mach number, 1.188.

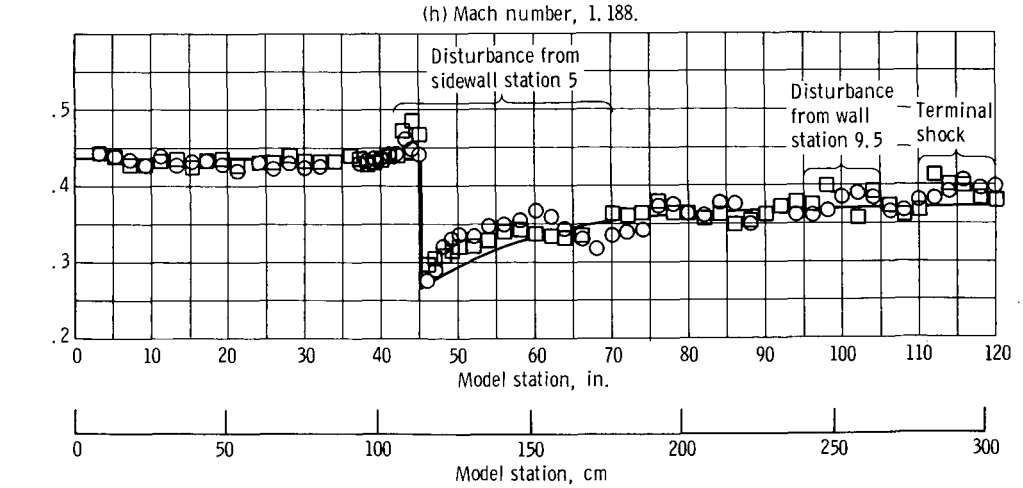

(i) Mach number, 1.271.

Figure 11. - Continued.

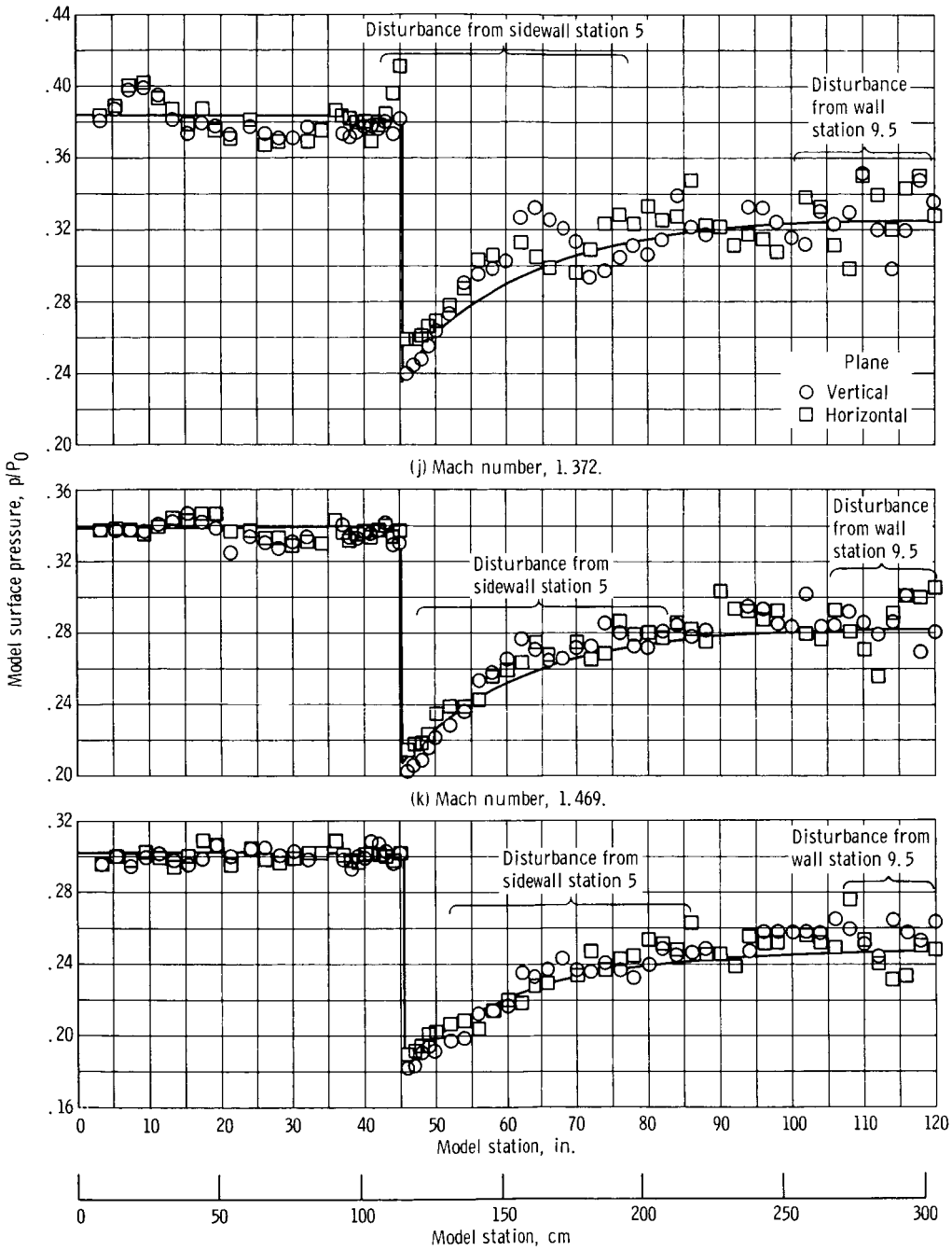

(j) Mach number, 1.372.

(k) Mach number, 1.469.

(l) Mach number, 1.558.

Figure 11. - Continued.

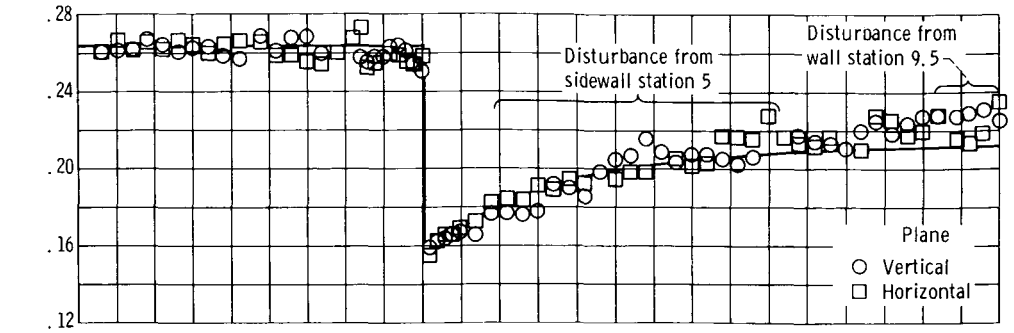

(m) Mach number, 1.659.

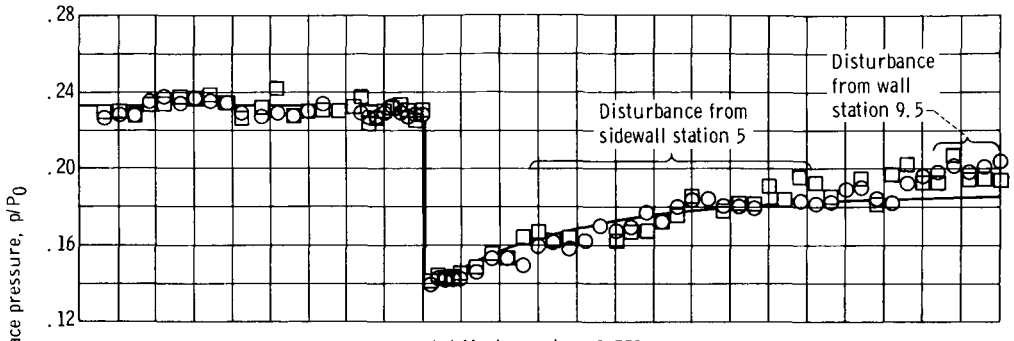

(n) Mach number, 1.750.

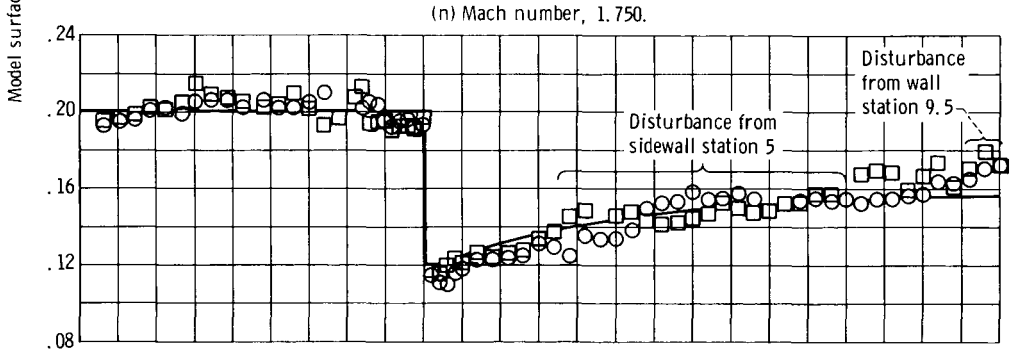

(o) Mach number, 1.861.

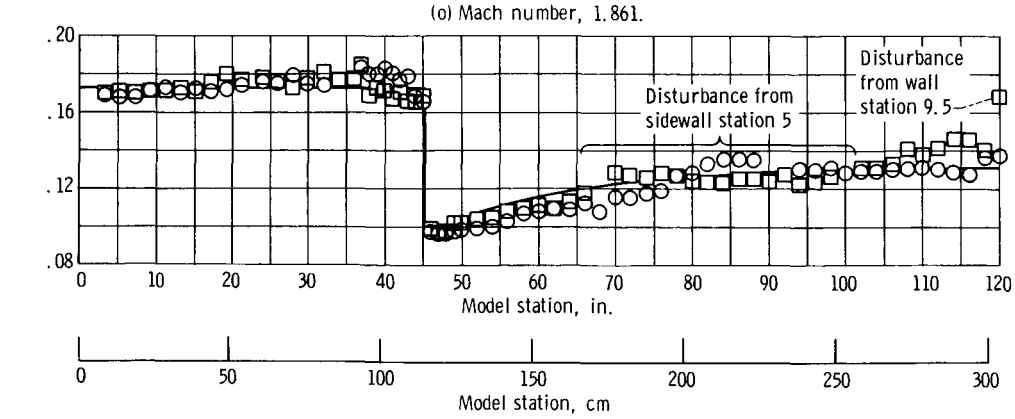

(p) Mach number, 1.970.

Figure 11. - Concluded.

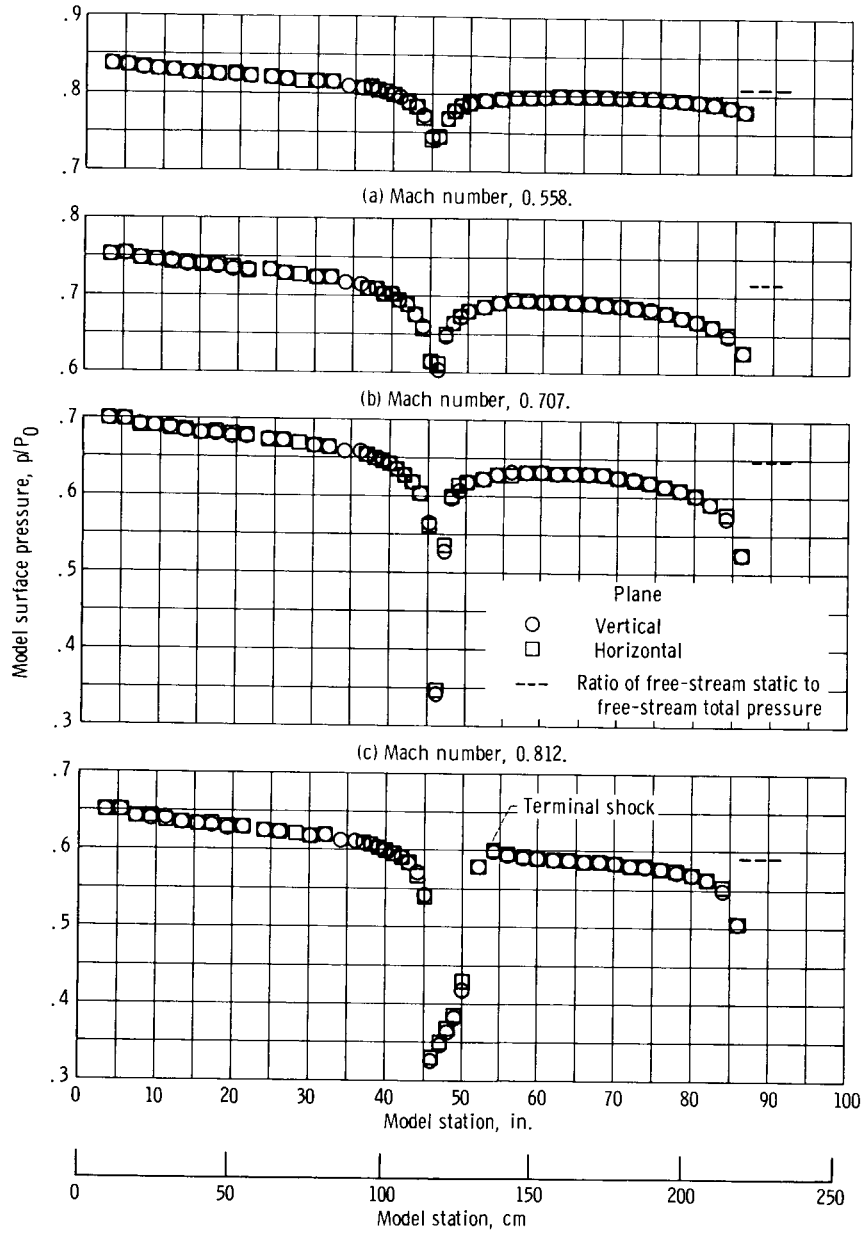

Figure 12. - Pressure distributions on 16-inch (40.64-cm) diameter 10° half-angle cone-cylinder model in 8-foot (2.44-m) - 6.2-percent porosity test section.

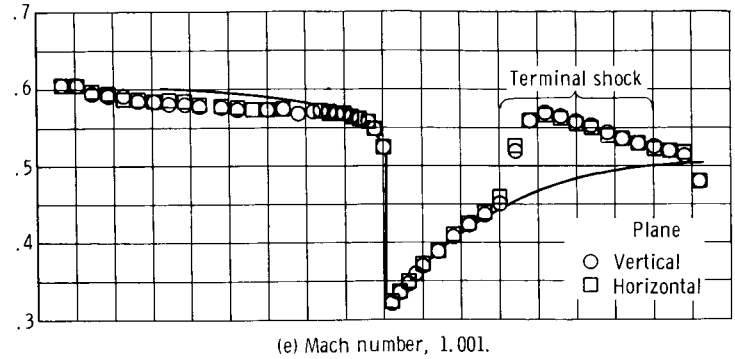

(e) Mach number, 1.001.

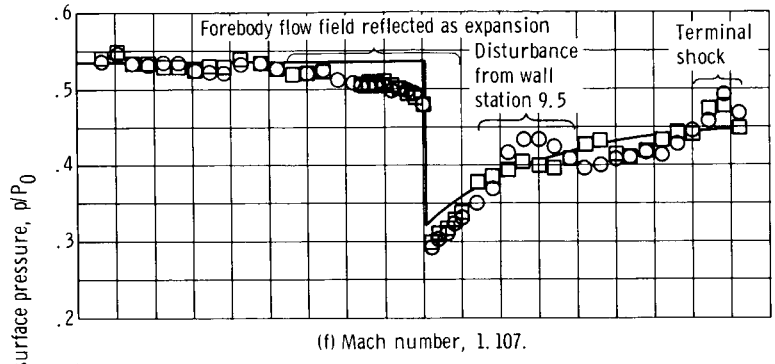

(f) Mach number, 1.107.

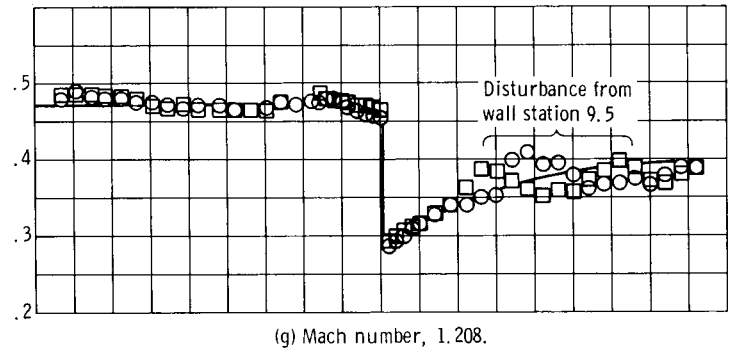

(g) Mach number, 1.208.

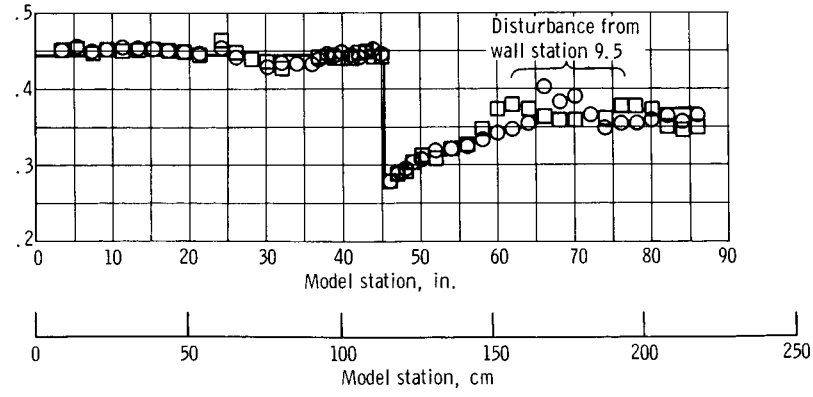

(h) Mach number, 1.255.

Figure 12. - Continued.

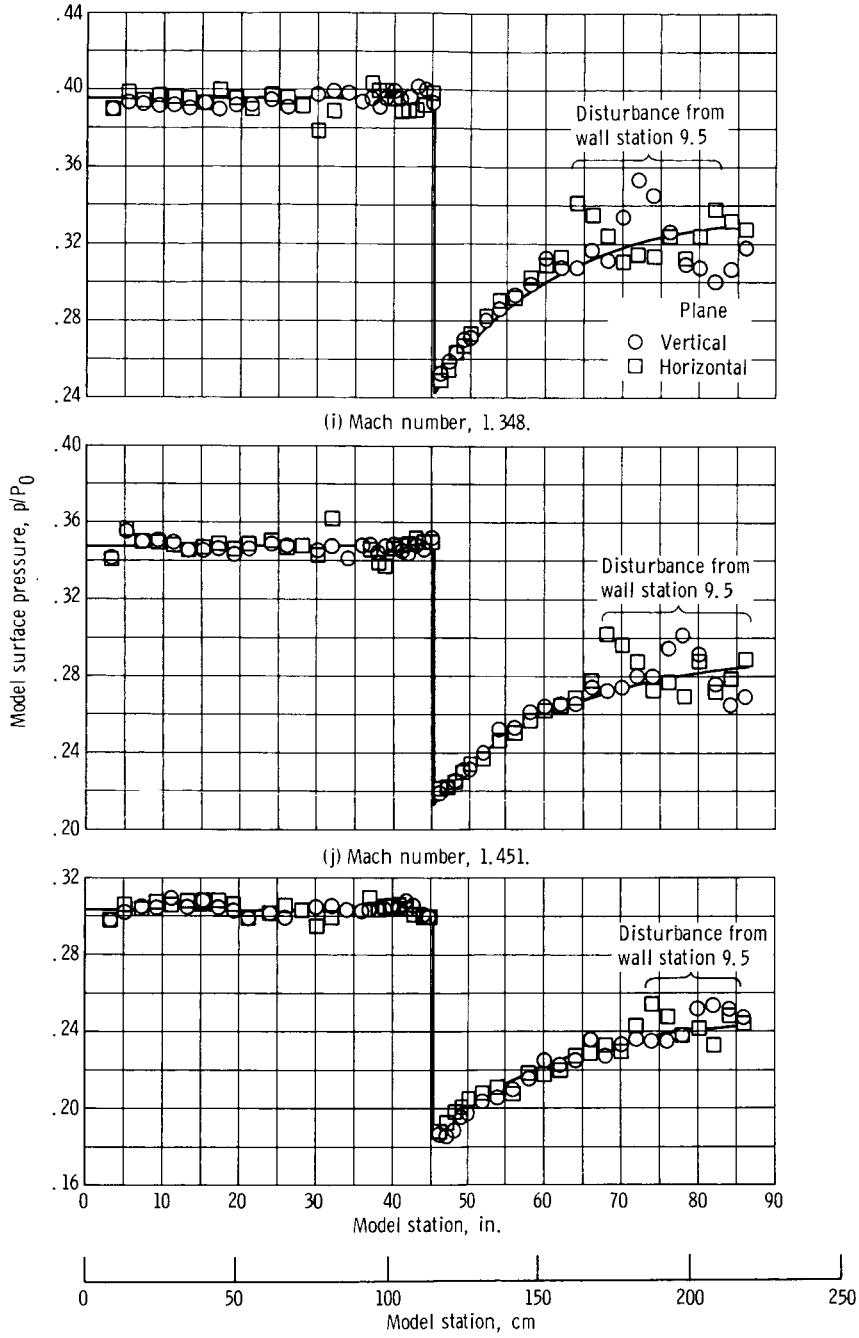

(k) Mach number, 1.555.

Figure 12. - Continued.

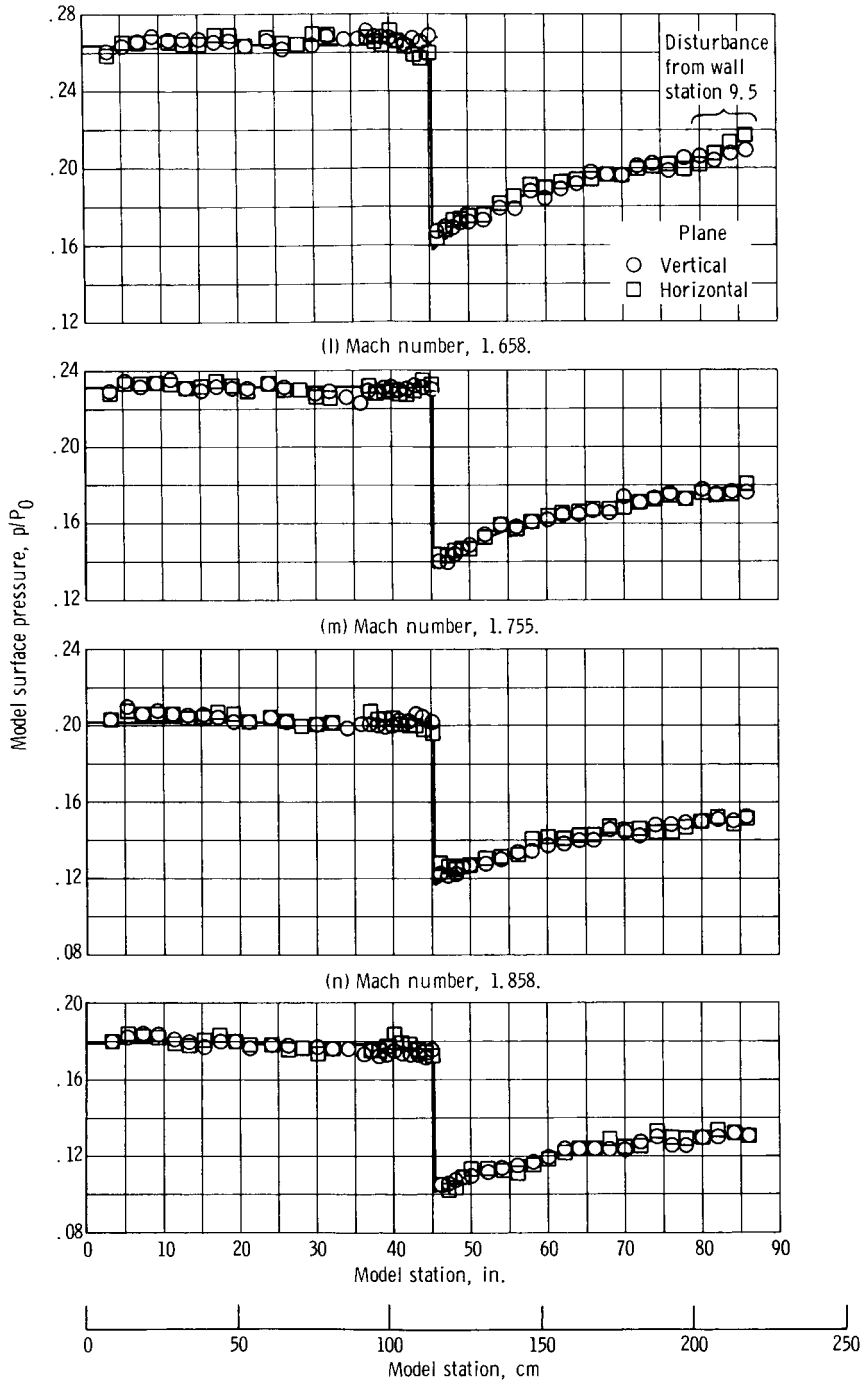

(l) Mach number, 1.658.

(m) Mach number, 1.755.

(n) Mach number, 1.858.

(o) Mach number, 1.944.

Figure 12. - Concluded.

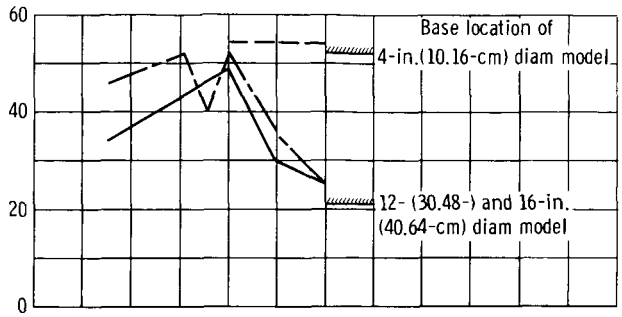

(a) Models in 14 foot (4.27 m) - 5.8-percent porosity test section.

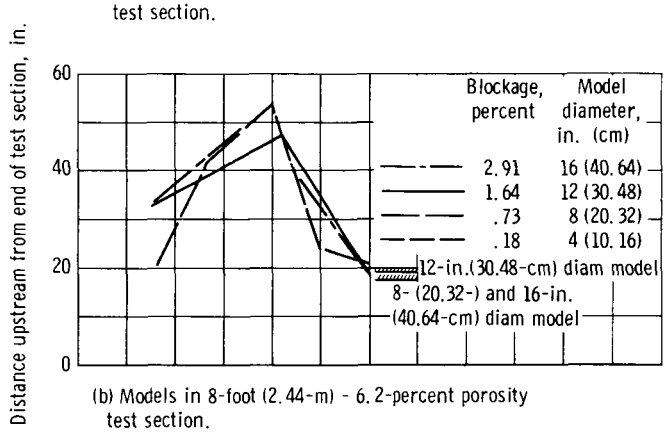

(b) Models in 8-foot (2.44-m) - 6.2-percent porosity test section.

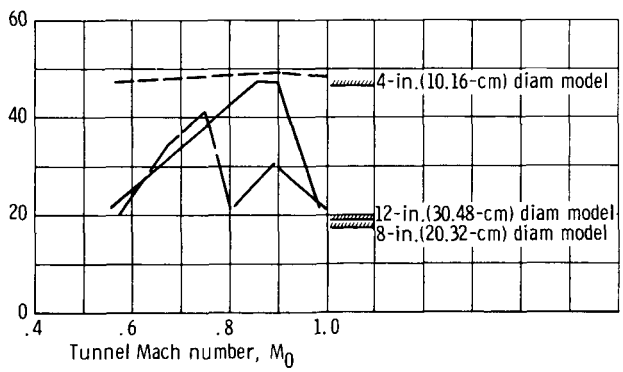

(c) Models in 8-foot (2.44-cm) - 3.1-percent porosity test section.

Figure 13. - Distance from end of test section upstream to model surface pressure decrease of 1 percent.

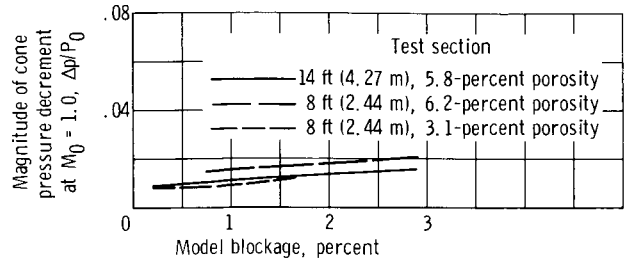

Figure 14. - Effect of model blockage on cone pressure decrement at Mach number 1.

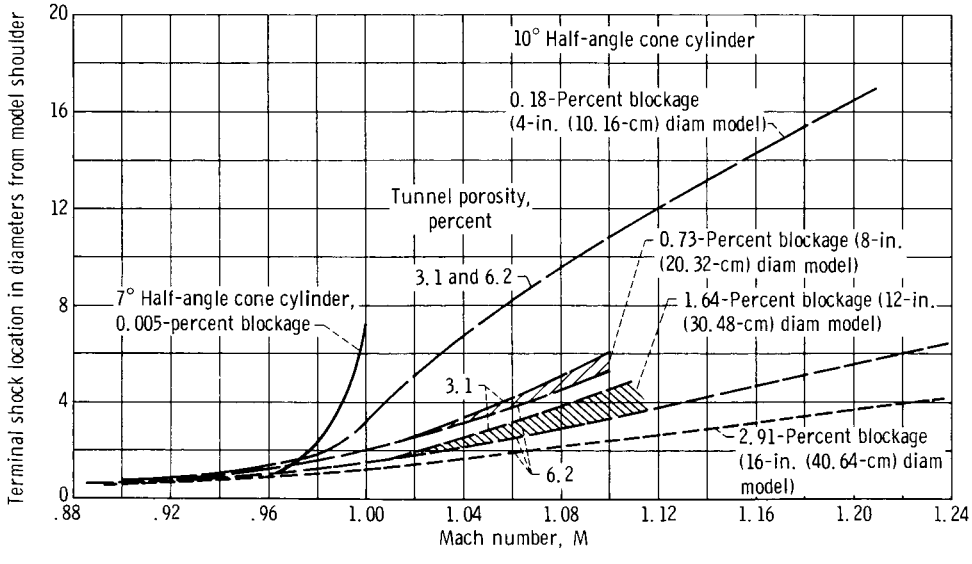

Figure 15. - Effect of blockage ratio on model terminal shock location.

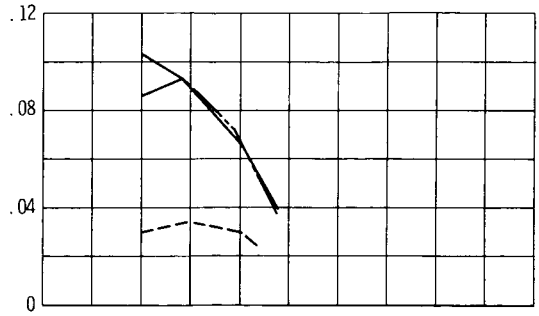

(a) Models in 14-foot (4.27-m) - 5.8-percent porosity test section.

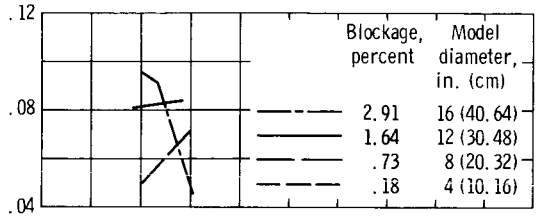

(b) Models in 8-foot (2.44-m) - 6.2-percent porosity test section.

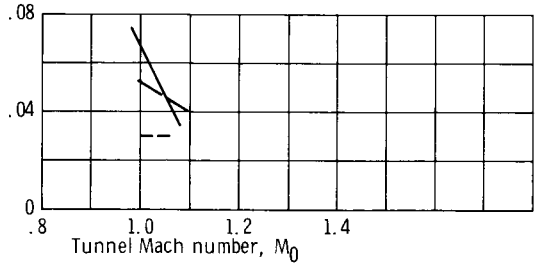

(c) Models in 8-foot (2.44-m) - 3.1-percent porosity test section.

Figure 16. - Effect of blockage on terminal shock magnitude.

Terminal shock disturbance magnitude, $\Delta p/P_0$

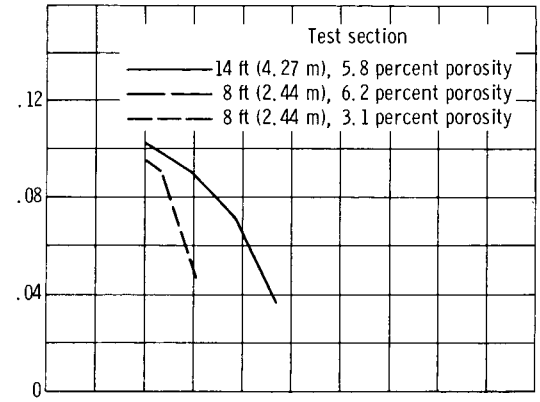

(a) 2.91-Percent blockage, 16-inch (40.64-cm) diameter model.

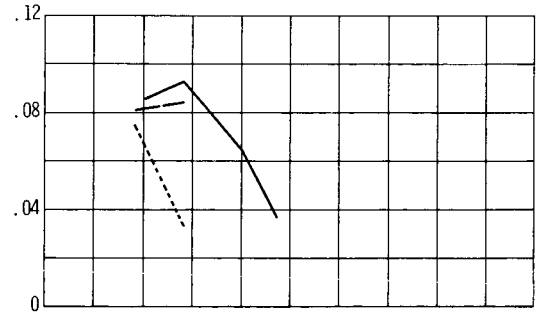

(b) 1.64-Percent blockage, 12-inch (30.48-cm) diameter model.

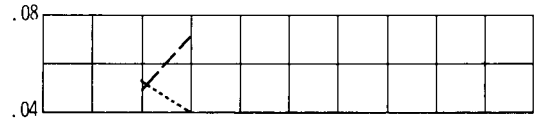

(c) 0.73-Percent blockage, 8-inch (20.32-cm) diameter model.

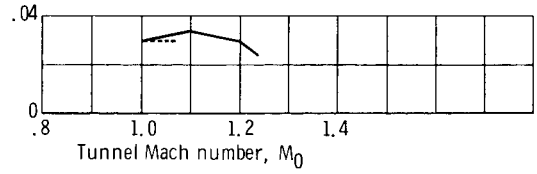

(d) 0.18-Percent blockage, 4-inch (10.16-cm) diameter model.

Figure 17. - Effect of test section configuration on terminal shock magnitude.

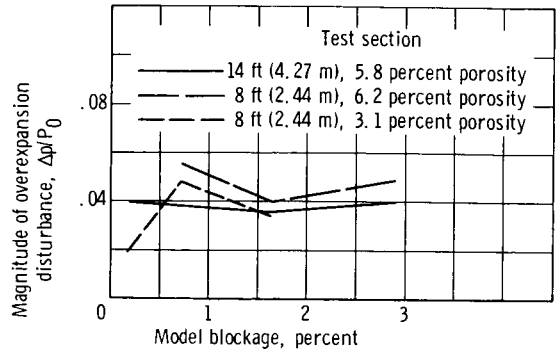

Figure 18. - Effect of blockage on overexpansion at $M_0 = 1.1$.

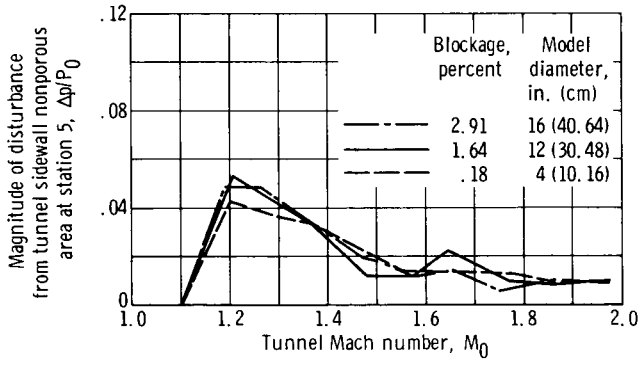

Figure 19. - Disturbance from sidewall nonporous area in 14-foot (4.27 m) test section.

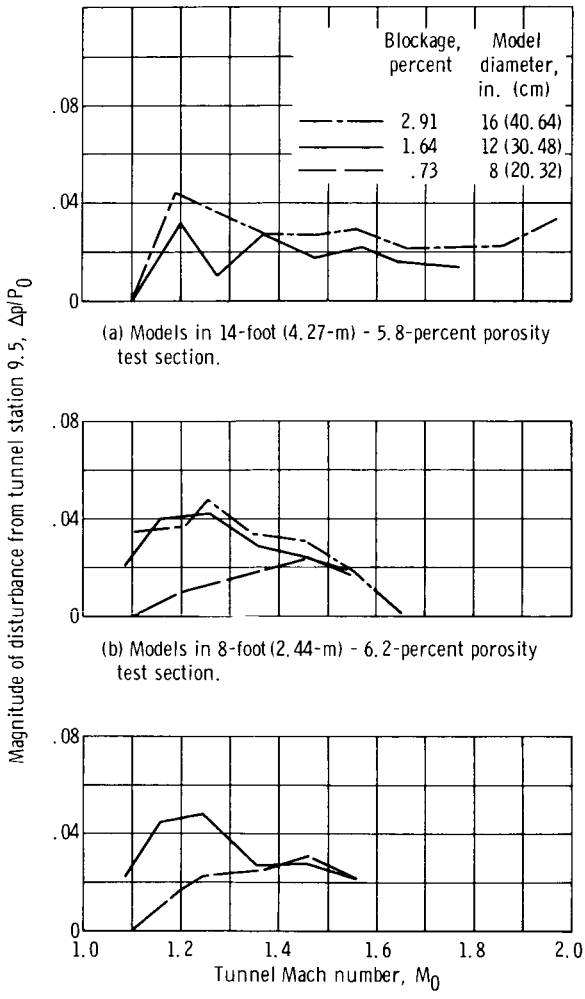

(a) Models in 14-foot (4.27-m) - 5.8-percent porosity test section.

(b) Models in 8-foot (2.44-m) - 6.2-percent porosity test section.

(c) Models in 8-foot (2.44-m) - 3.1-percent porosity test section.

Figure 20. - Effect of model blockage on disturbance from tunnel station 9.5.

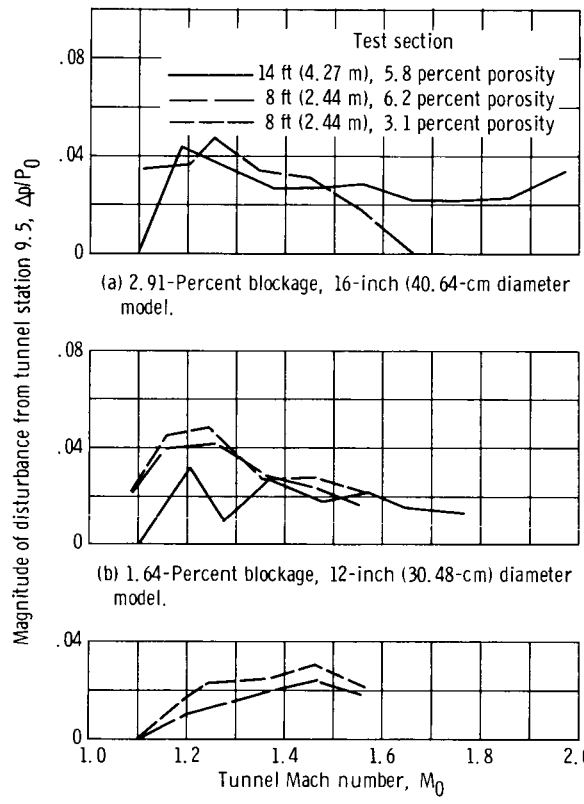

(a) 2.91-Percent blockage, 16-inch (40.64-cm diameter model.

(b) 1.64-Percent blockage, 12-inch (30.48-cm) diameter model.

(c) 0.73-Percent blockage, 8-inch (20.32-cm) diameter model.

Figure 21. - Effect of test section configuration on disturbance from tunnel station 9.5.

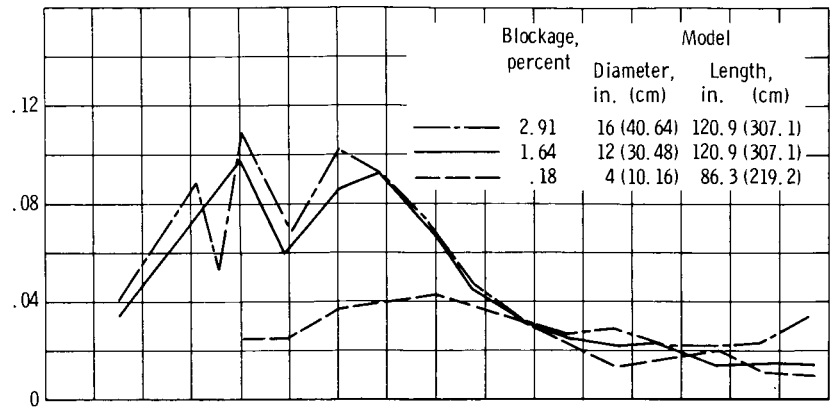

(a) Models in 14-foot (4.27-m) - 5.8-percent porosity test section.

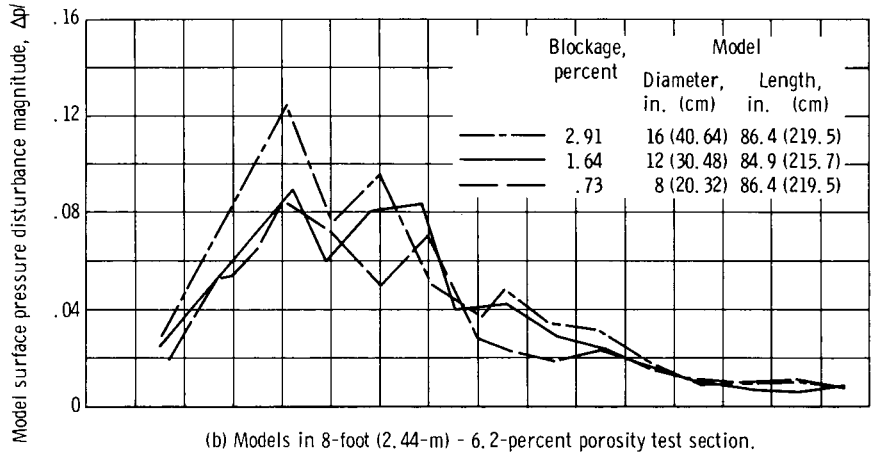

(b) Models in 8-foot (2.44-m) - 6.2-percent porosity test section.

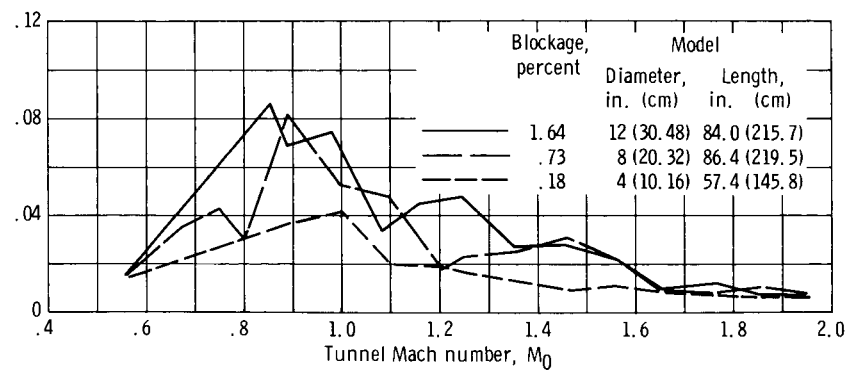

(c) Models in 8-foot (2.44-m) - 3.1-percent porosity test section.

Figure 22. - Effect of blockage on model surface pressure disturbances.

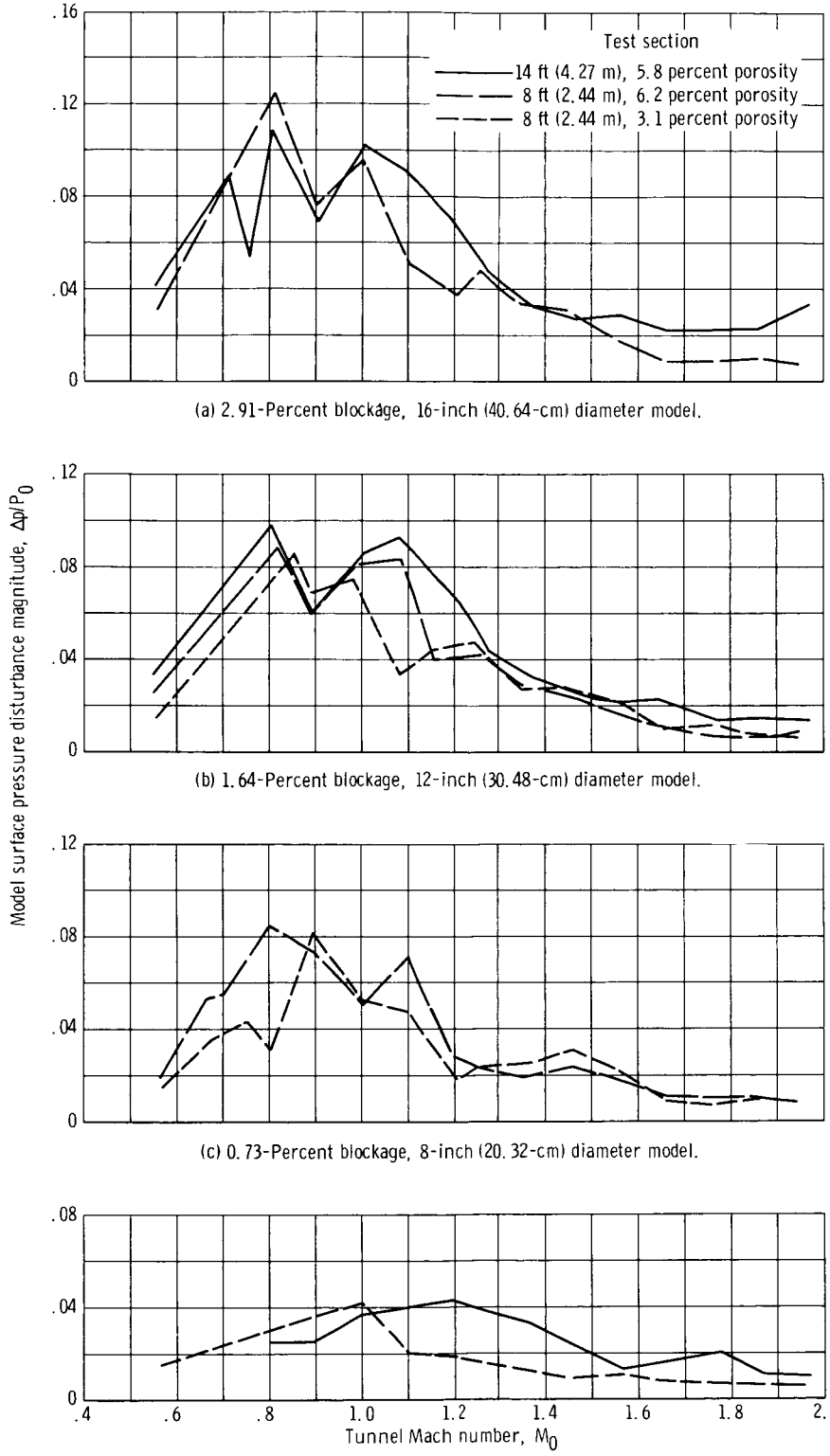

(a) 2.91-Percent blockage, 16-inch (40.64-cm) diameter model.

(b) 1.64-Percent blockage, 12-inch (30.48-cm) diameter model.

(c) 0.73-Percent blockage, 8-inch (20.32-cm) diameter model.

(d) 0.18-Percent blockage, 4-inch (10.16-cm) diameter model.

Figure 23. - Effect of test section configuration on model surface pressure disturbances.

(a) 2.91-Percent blockage, 16-inch (40.64-cm) diameter model.

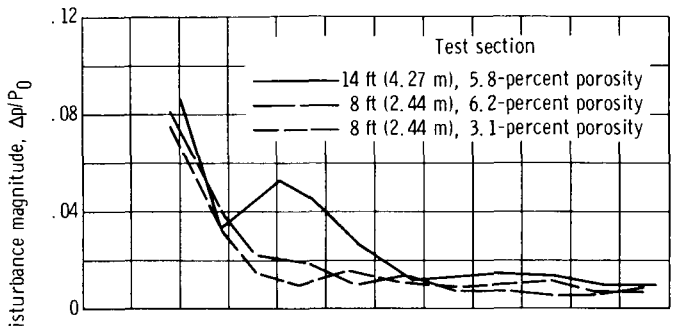

(b) 1.64-Percent blockage, 12-inch (30.48-cm) diameter model.

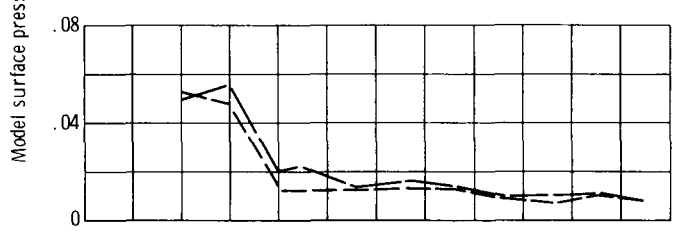

(c) 0.73-Percent blockage, 8-inch (20.32-cm) diameter model.

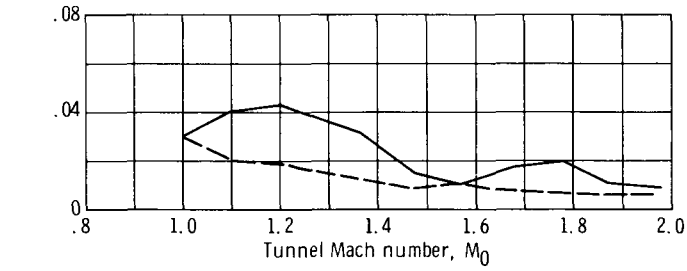

(d) 0.18-Percent blockage, 4-inch (10.16-cm) diameter model.

Model surface pressure disturbance magnitude, $\Delta p/P_0$

Figure 24. - Effect of test section configuration on model surface pressure disturbances within 57 inches (145 cm) of model nose.

NASA-Langley, 1968 — 1 E-4399